AD-A039 766 BOSTON COLL CHESTNUT HILL MASS SPACE DATA ANALYSIS LAB F/G 19/7
ATTITUDE DETERMINATION SYSTEM FOR ROCKETS USING GYROSCOPIC PLAT--ETC(U)
OCT 76 B F SULLIVAN, M E STICK F19628-75-C-0045
UNCLASSIFIED BC-SDAL-76-4A AFGL-TR-76-0310 NL

1 OF 1
AD A039766

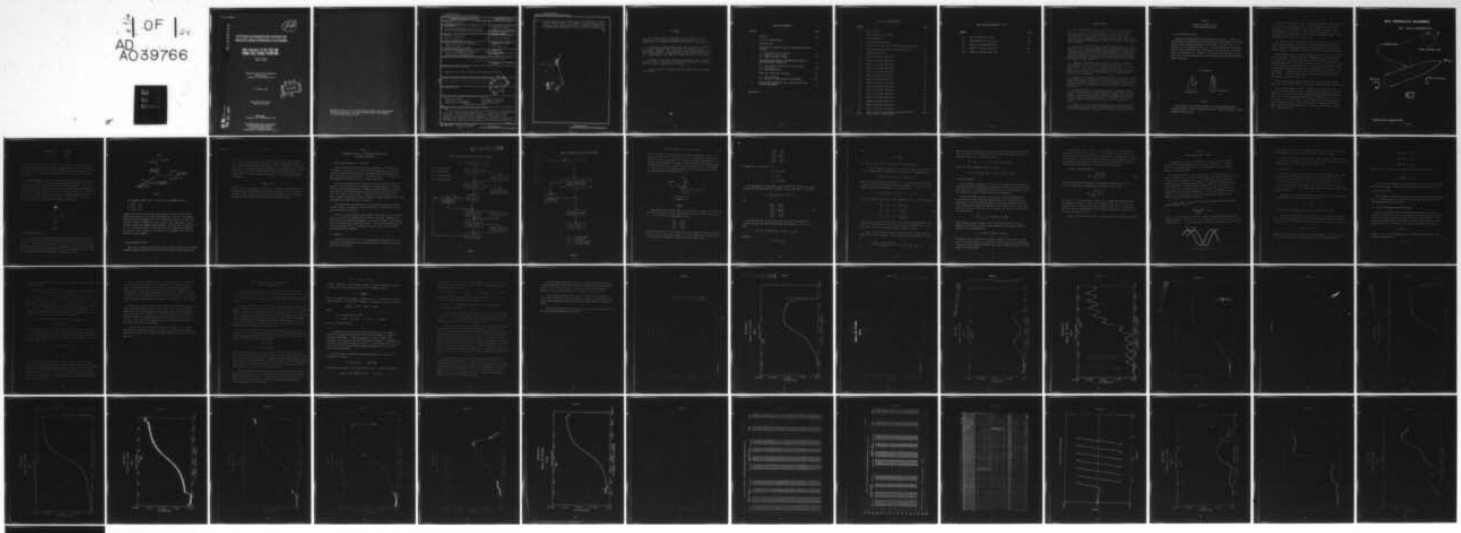

END

DATE FILMED
6-77

AFGL-TR-76-0310

AD A039766

12 p. 5.

ATTITUDE DETERMINATION SYSTEM FOR ROCKETS USING GYROSCOPIC PLATFORMS

COPY AVAILABLE TO DDC DOES NOT PERMIT FULLY LEGIBLE PRODUCTION

Brian F. Sullivan
Marvin E. Stick

SPACE DATA ANALYSIS LABORATORY
Boston College
Chestnut Hill, Massachusetts 02167

DDC
RECEIVED
APR 28 1976
C

31 October 1976

Approved for public release;
distribution unlimited

AD No.
DDC FILE COPY

Final Report
1 November 1974 - 30 September 1976

AIR FORCE GEOPHYSICS LABORATORY
AIR FORCE SYSTEMS COMMAND
UNITED STATES AIR FORCE
HANSCOM AFB, MASSACHUSETTS 01731

Qualified requestors may obtain additional copies from the Defense Documentation Center. All others should apply to the National Technical Information Service.

UNCLASSIFIED

SECURITY CLASSIFICATION OF THIS PAGE (When Data Entered)

(19) REPORT DOCUMENTATION PAGE	READ INSTRUCTIONS BEFORE COMPLETING FORM
1. REPORT NUMBER (18) AFGL-TR-76-0310 ✓	2. GOVT ACCESSION NO.
3. RECIPIENT'S CATALOG NUMBER	
4. TITLE (and Subtitle) (6) ATTITUDE DETERMINATION SYSTEM FOR ROCKETS USING GYROSCOPIC PLATFORMS.	5. TYPE OF REPORT & PERIOD COVERED Final Scientific 1 Nov 74 - 30 Sept 76
	6. PERFORMING ORG. REPORT NUMBER (14) BC-SDAL-76-4A ✓
7. AUTHOR(s) (10) Brian F. Sullivan / Marvin E. Stick	8. CONTRACT OR GRANT NUMBER(s) (15) F19628-75-C-0045 ✓
9. PERFORMING ORGANIZATION NAME AND ADDRESS Space Data Analysis Laboratory ✓ Boston College Chestnut Hill, Ma. 02167	10. PROGRAM ELEMENT, PROJECT, TASK AREA & WORK UNIT NUMBERS 62301E 9993 T&WU n/a
11. CONTROLLING OFFICE NAME AND ADDRESS Air Force Geophysics Laboratory Hanscom AFB, Massachusetts Monitor/Paul Tsipouras/SUA	12. REPORT DATE (11) 31 Oct 76
	13. NUMBER OF PAGES 53
14. MONITORING AGENCY NAME & ADDRESS (if different from Controlling Office) (12) 54 p.	15. SECURITY CLASS. (of this report) Unclassified
	15a. DECLASSIFICATION/DOWNGRADING SCHEDULE

16. DISTRIBUTION STATEMENT (of this Report)

Approved for Public Release; Distribution Unlimited

17. DISTRIBUTION STATEMENT (of the abstract entered in Block 20, if different from Report)

(9) Final rept. 1 Nov 74 - 30 Sep 76

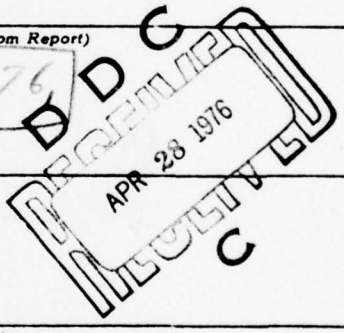

18. SUPPLEMENTARY NOTES

19. KEY WORDS (Continue on reverse side if necessary and identify by block number)

Rocket Attitude
Gyroscopic Platforms
Gyroscopic Measurements
Attitude Calculation
Refinement Techniques
Data Simulation
Correction Procedures

20. ABSTRACT (Continue on reverse side if necessary and identify by block number)

The system used to calculate the attitude of a rocket whose principal attitude measuring system is a gyroscopic platform is discussed. The various types of gyro systems, their comparisons and differences are presented. A synopsis of the mathematical analysis used to compute the attitude is displayed. Various data refinement techniques and correction procedures for

(cont.)

DD FORM 1 JAN 73 1473 EDITION OF 1 NOV 65 IS OBSOLETE

403 460

UNCLASSIFIED

SECURITY CLASSIFICATION OF THIS PAGE (When Data Entered)

20. rockets whose systems malfunction are presented. Results in the form of plots of the angle of attack between the velocity vector and rocket axis for several rockets whose attitudes were determined by this system are exhibited.

PREFACE

The authors wish to thank Mr. Leo F. Power, Jr., the Director of the Space Data Analysis Laboratory, for his administrative assistance during the period of this contract.

Analysis and programming assistance was capably provided by several members of the laboratory. We wish to thank Mr. Paul E. Connolly, Mr. Robert Raistrick, Mr. Leonard Marino, Miss Meghan Hurley. Thanks also go to Mr. Dennis Delorey, Mr. Joseph Martine, Mr. Paul N. Pruneau and Mrs. Carol Foley.

We wish to thank our Contract Monitors, Mr. Paul Tsipouras and Mr. Robert E. McInerney of Analysis and Simulation Branch (SUA) for their guidance and assistance.

Finally, special thanks go to Miss Mary Kelly for typing this report.

TABLE OF CONTENTS

LIST OF ILLUSTRATIONS

LIST OF ILLUSTRATIONS (Cont.)

INTRODUCTION

The orientation of the sensing axis of an instrument with respect to a fixed coordinate system in space is referred to as its attitude. From the attitude of a sensor, one may determine the angle it makes with any other vector such as the rocket's velocity vector, the sun line vector, etc. For certain sensors, meaningful interpretation of the instrument's output can be accomplished only when the attitude of the sensor axis is known.

The first section of this report discusses various types of gyroscopic platforms used as attitude measuring systems on vehicles. The systems include the Attitude Control System with two free gyros, the Miniature Attitude Reference System with segmented lengths over a 5 volt span for the roll, pitch and yaw axes, and the Miniature Inertial Digital Attitude System with a one-to-one correspondence between angular displacements and digital coding outputs.

The next discussion centers upon processing procedures which produce final attitude information from vehicle gyro measurements. An analysis is shown which relates any onboard probe vector $\hat{P}$ to the local coordinate system fixed at the launch site. With the orientation of $\hat{P}$ determined, the attack angle with any other attitude determined or predetermined vector can be supplied.

To provide continuous final output for the attitude system measurements, data refinements techniques are introduced with statistical error bound values on the predicted versus measured output. Tolerance levels are set on the measured input data to ensure that all predicted data will be within a specified σ deviation.

Oftentimes the initial orientations of onboard sensors require corroboration. A phase and time shift study is introduced in the third section to compare the phase relationship between measured and attitude predicted magnetometer pitch angles during well-behaved areas of a vehicle's flight. The routines can be used for both side and axial magnetometer output.

Finally, some of the more common types of problems with gyro systems are discussed. The correction procedures used on these malfunctions are discussed and the results exhibited.

SECTION 1

GYROSCOPIC PLATFORMS USED AS ATTITUDE MEASURING SYSTEMS

1.1 Attitude Control System

Space Vector Corporation's Attitude Control System (ACS) is comprised of a Roll Stabilized Platform (RSP) with two free gyros which output a yaw, pitch and roll vehicle motion from top dead center (TDC) of the gyro. TDC is the reference for all onboard probes (Fig. 1). The roll and yaw are true measurements of vehicle motion but since there are only two free gyros, true vehicle pitch is a function of yaw. Further, if the vehicle yaws over 85°, this will cause loss of initial reference for the system and make attitude determination almost impossible.

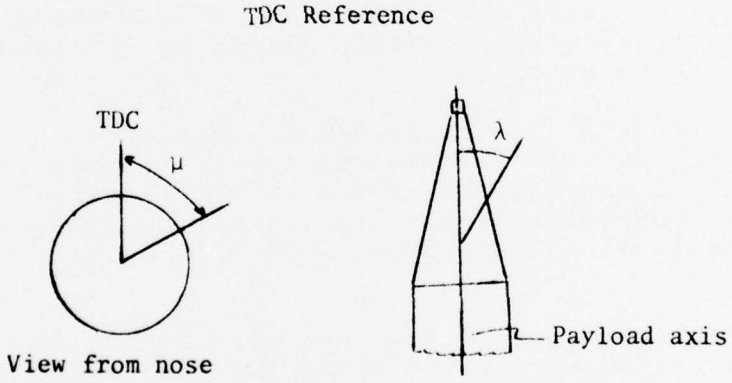

Figure 1

Various models of the ACS were used as attitude measuring systems on vehicles analyzed. They all function similarly but output differently. Typical examples are given below.

Model 10580 ACS flown on IC630.02-1A output pitch coarse, pitch fine, yaw coarse, yaw fine, and roll gyro data. The pitch and yaw coarse data were calibrated in .12 volt increments with a linear conversion range of ±90° corresponding to a 5 volt span. The pitch and yaw fine data over a similar volt span had a conversion range of ±5°. The roll telemetry data had a linear conversion range of ±180° on a 4.8 volt span.

According to Figure 2, pitch coarse for this model was decreasing voltage output when pitching down, pitch fine was increasing voltage when pitching down. A yaw right motion was increasing yaw coarse voltage and a decreasing yaw fine voltage. A clockwise roll viewed aft to nose was increasing voltage.

Model 10390 ACS flown on IC519.07-1B output only pitch coarse, yaw coarse and roll gyro data. The pitch data was calibrated over a ±90° corresponding to a 5 volt span. However, to model the calibration information, discrete polynomial expressions were used over finite intervals. From 0 volts - 4 volts, a linear model was used and from 4 volts - 5 volts, a second degree model best represented the calibration information. The yaw data was converted to angle measurements in a fashion similar to that used for the coarse yaw output on model 10580. The roll telemetry data had a linear conversion range of four ±45° segments, each on a 5 volt span.

Pitch and yaw coarse output references were similar to those for model 10380, but clockwise roll output was decreasing voltage when viewed aft to nose.

Model 10550 ACS flown on A10.304-1 output pitch coarse, pitch fine, yaw coarse, yaw fine and roll gyro data. The pitch coarse segment was calibrated from -20° to +170° over a 5 volt span with decreasing voltage when pitching down. The yaw coarse segment was calibrated for a range of ±70° over a 3.3 volt span, i.e., .8 to 4.1 volts. A yaw right motion was decreasing voltage for the coarse yaw output. Three data points were recorded for pitch fine data, and the curve connecting each pair of points is essentially a straight line. These points are:

ACS COORDINATE REFERENCE

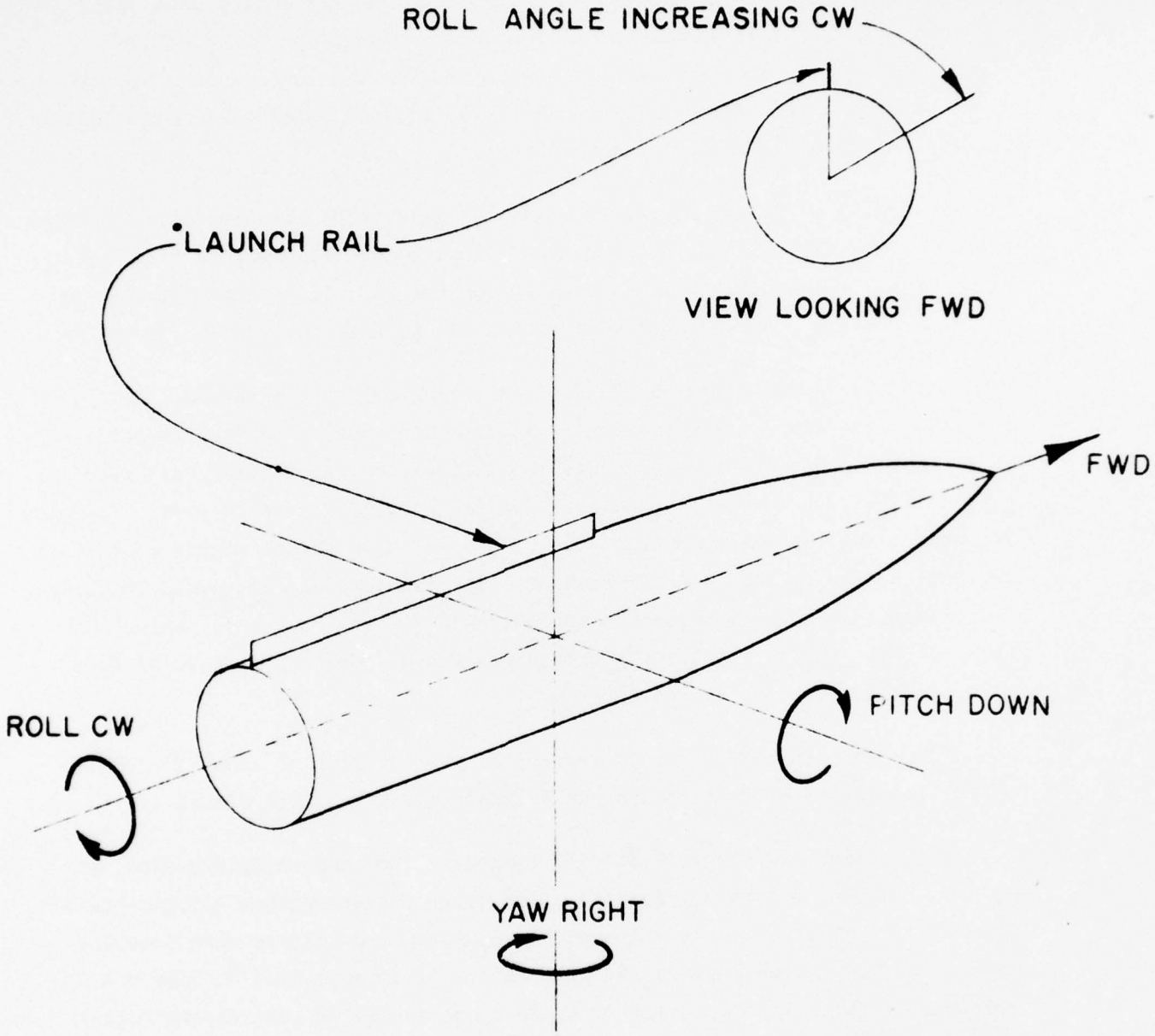

•LAUNCH RAIL = 0 degrees ROLL

Figure 2

Angle (Deg.)	Voltage
-1	0.41
0	3.20
+1	4.32

No data calibration points were recorded for yaw fine. According to Figure 2, pitch fine was increasing voltage when pitching down and yaw fine was increasing voltage when yaw to the right. The roll segment was calibrated from 180° CCW to 178° CW over a 4.7 volt span with voltage decreasing for a CW roll when viewed aft to nose.

Another ACS gyro reference system was the Space Data Corporation system used for the vehicle EX531.43-1. The pitch and yaw channel output were ±180° over a 5 volt span and the roll channel output was a 360° segment over a 5 volt span. Although not used in the data reduction, the pitch and yaw high resolution were ±10°. The zero reference for the gyro roll was the launch rail (Figure 3). Gyro pitch zero was 73.3° launcher elevation setting at gyro uncage and gyro yaw zero was 46.2° launcher azimuth setting at gyro uncage. Looking forward, yaw right is positive, pitch up is negative and roll clockwise is positive.

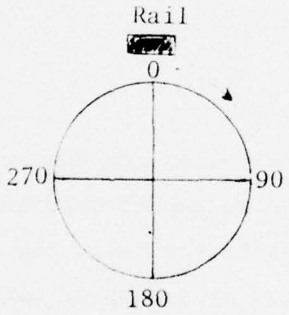

Figure 3

1.2 MARS Attitude System

The Space Vector Corporation's Miniature Attitude Reference System (MARS) provided gyroscopic output for the determination of rocket attitude for the vehicle A10.302-1. The roll axis coincided with the rocket axis at launch and the orientation of a gyro reference notch was used to determine the location of the yaw axis. The cross product of the yaw axis with the roll axis yielded the pitch axis. The axes and rotations of the MARS system are identified in Figure 4.

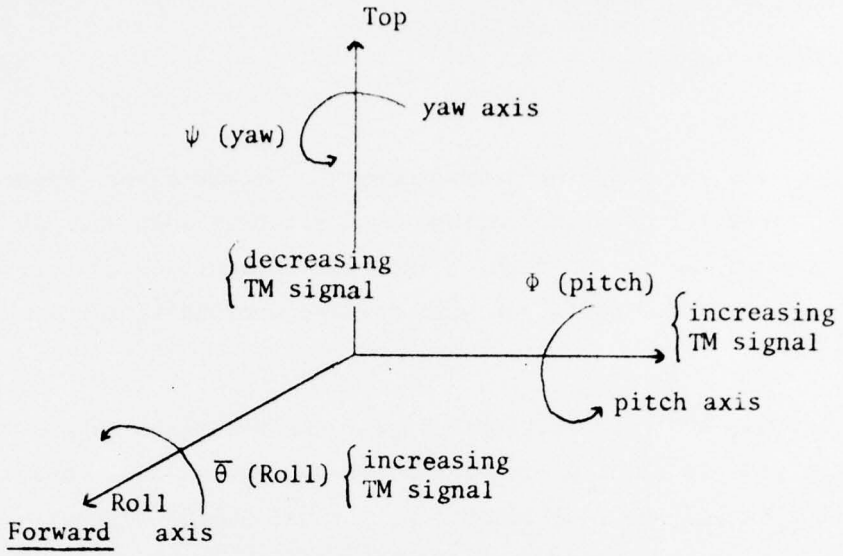

Figure 4

The segmented lengths over a 5 volt span for each MARS axis are:

a) Roll: 90°
b) Yaw: 60°
c) Pitch: 45°.

Segment identification of the pitch and yaw outputs for this system requires continuous monitoring of the output to determine the instance of instantaneous transitions from one segment to the next. By keeping track of the transitions and their direction evidenced by a plus or minus 5 volt step change, one may correctly identify the segments being presented. The roll output identification was a 5° ±3° shorted segment in the center of the 1st segment which appeared as a constant output voltage for that portion of the segment. This short was repeated every 4th segment.

1.3 MIDAS Attitude System

Space Vector Corporation's Miniature Inertial Digital Attitude System (MIDAS) provided gyroscopic output used to calculate the attitude of many rockets such

as A10.403-3. The roll, pitch and yaw references are the same as for a MARS system but the outputs differ considerably. Whereas a MARS system outputs in a 5 volt span representing some degree segment having a predetermined length, the MIDAS system's roll, pitch and yaw measurements are digitized by optical encoders and result in a one-to-one correspondence between angular displacements and digital codings. For the digital coding variable n, the angular displacement ϕ in degrees is

$$\phi = \frac{n}{1024} \times 360 \ .$$

No bias values are needed for conversion since the MIDAS system represents the displacement from the uncaged position of the gyro which fixes the coordinate reference system. The flow of attitude data for MIDAS vehicles is simplified considerably when compared with the flow of ACS and MARS vehicles.

SECTION 2

PROCESSING PROCEDURES, MATHEMATICAL ANALYSIS, AND REFINEMENT TECHNIQUES

2.1 Processing Procedures for all Rockets

The oscillogram containing vehicle gyro measurements is inspected for calibrations, extreme noise, gyro malfunctions, approximate spin rates, precessional period and half cone angle. The digital tape containing the gyro data is then unpacked and converted to degrees and plotted. These plots are then compared with results of the oscillogram inspection.

If no gyro malfunction occurs then the quick-look attitude and angles of attack for the rocket axis are calculated based upon preliminary information. If the attitude measuring system is a MIDAS, then attack angles for requested side probes are calculated at the same time as attack angles for the rocket axis. If attitude for side probes is requested for an ACS or MARS syste..., the roll data is converted to degrees, checked for proper conversion and then the preliminary side probe attitude is calculated.

All extreme noise and calibrations are filtered from the gyro conversions and this output, if displaying a lack of continuity, is curve fitted by techniques discussed in Section 2.3.

Finally, if onboard probes measure magnetic field, lunar, or solar intensities, it is possible to corroborate the calculated attitude. Depending upon the accuracy of the onboard measurements, an error bar estimate of the attitude can be included as part of the normal output. A flow of the attitude data for both ACS and MARS vehicles is displayed in Figure 5, and a flow of the data for MIDAS vehicles in Figure 6.

2.2 Analysis

Given the unit vectors $\hat{X}$, $\hat{Y}$, $\hat{Z}$ in the directions of the gyro roll, pitch and yaw axes, the direction of the longitudinal axis of the vehicle can be expressed as the vector e''_r:

BEST AVAILABLE COPY

FLOW OF ATTITUDE DATA FOR ACS AND MARS VEHICLES

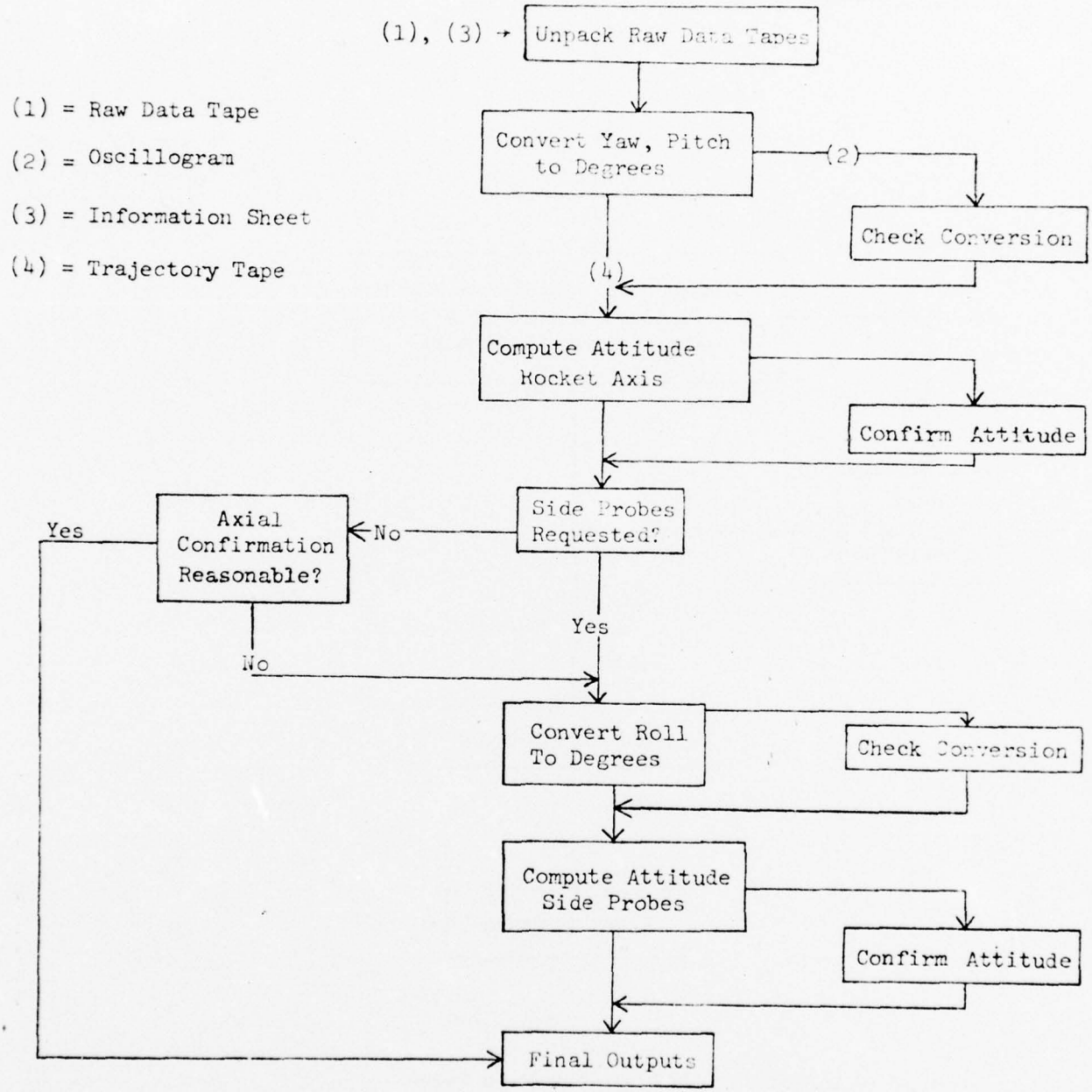

Figure 5

BEST AVAILABLE COPY

FLOW OF ATTITUDE DATA FOR MIDAS VEHICLES

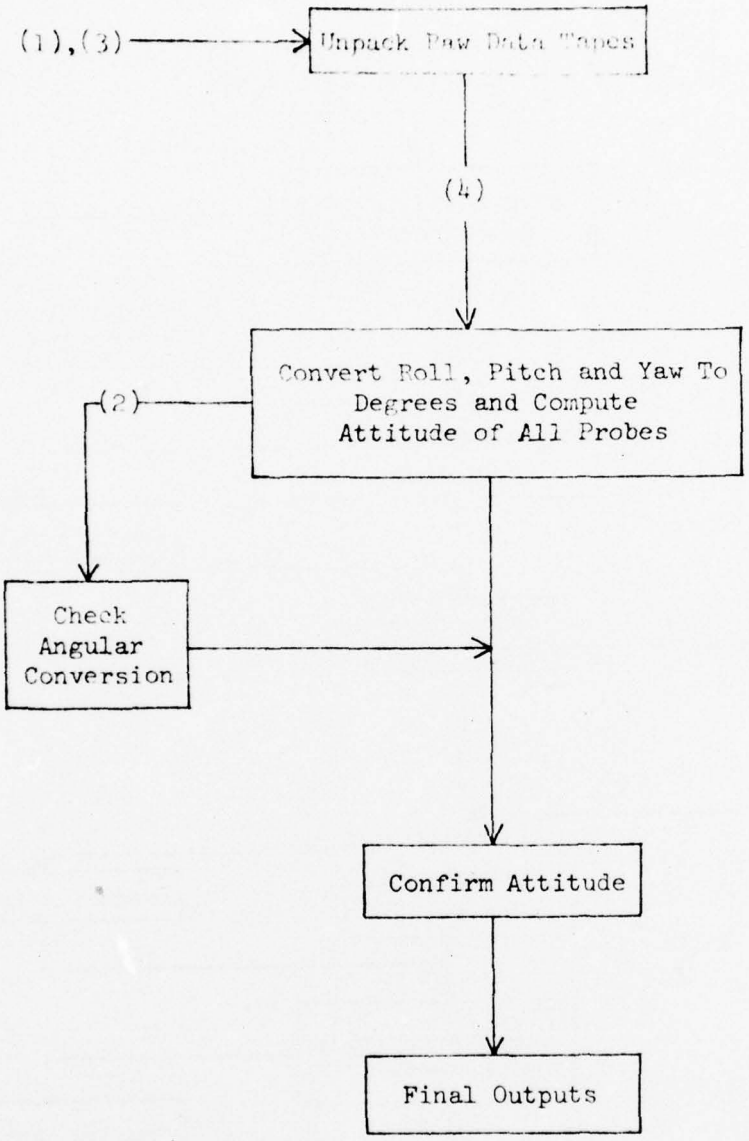

(1) = Raw Data Tape
(2) = Oscillogram
(3) = Information Sheet
(4) = Trajectory Tape

Figure 6

$$e''_r = \hat{X} \cos y \cos p + \hat{Y} \sin y + \hat{Z} \cos y \sin p \qquad (2.1)$$

where y and p are the true vehicle yaw and pitch respectively. Now let e_{θ_c}, e_{ϕ_c}, e_{r_c} be unit vectors in the directions of true North, East and the local vertical, fixed at the launch site. Within this system, the elevation of a vector may be determined as the angle it makes with the local horizontal plane with the direction of the vertical taken as positive elevation. The azimuth of a vector is the angle between its projection in the horizontal plane and e_{θ_c} measured positive clockwise (see Fig. 7).

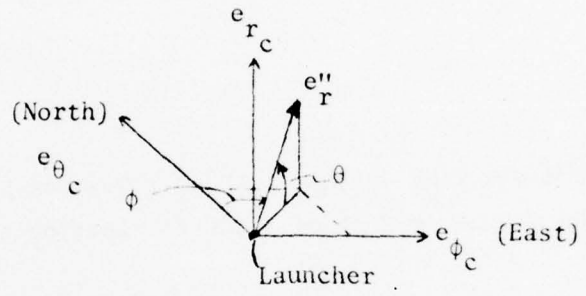

θ = Elevation of e''_r

ϕ = Azimuth of e''_r

Figure 7

Using the direction coefficients of the gyro axes at launch, the unit vectors $\hat{X},\hat{Y},\hat{Z}$ can be expressed as linear combinations of the earth-based system $e_{\theta_c}, e_{\phi_c}, e_{r_c}$. If we call the coefficient matrix B, then

$$\begin{bmatrix} \hat{X} \\ \hat{Y} \\ \hat{Z} \end{bmatrix} = B \begin{bmatrix} e_{\theta_c} \\ e_{\phi_c} \\ e_{r_c} \end{bmatrix} .$$

According to equation (6) of Reference [3], we can define a system of orthonormal vectors e''_r, e''_1, e''_2 at any time in flight as a linear combination of the gyro axes. If A represents the coefficient matrix of the gyro output, then

$$\begin{bmatrix} e''_r \\ e''_1 \\ e''_2 \end{bmatrix} = A \begin{bmatrix} \hat{X} \\ \hat{Y} \\ \hat{Z} \end{bmatrix} .$$

In particular, as described in (2.1)

$$a_{11} = \cos y \cos p$$

$$a_{12} = \sin y$$

$$a_{13} = \cos y \sin p .$$

To transform the time dependent e''_r, e''_1, e''_2 system into the local $e_{\theta_c}, e_{\phi_c}, e_{r_c}$ system, form the matrix product of A and B. Letting the matrix C = AB, then

$$c_{ij} = \sum_{m=1}^{3} a_{im} b_{mj} \quad (i,j = 1,2,3)$$

and

$$\begin{bmatrix} e''_r \\ e''_1 \\ e''_2 \end{bmatrix} = C \begin{bmatrix} e_{\theta_c} \\ e_{\phi_c} \\ e_{r_c} \end{bmatrix} . \qquad (2.2)$$

Once the attitude of the vehicle's main axis has been determined as direction cosines, the elevation and azimuth may be derived. From (2.2); we have:

$$e''_r = e_{\theta_c} \cos\theta \cos\phi + e_{\phi_c} \cos\theta \sin\phi + e_{r_c} \sin\theta .$$

Therefore:

$$\theta = \sin^{-1} (c_{13}) ,$$

and

$$\phi = \tan^{-1}\left(\frac{c_{12}}{c_{11}}\right) .$$

The elevation and azimuth of e_1'' and e_2'' are similarly derived.

In order to extend this approach to a vector $\hat{P}$ lying in the sensing direction of a probe having any orientation on the rocket, $\hat{P}$ is represented as

$$\hat{P} = e_r'' \cos\lambda + e_1'' \cos\mu \sin\lambda + e_2'' \sin\mu \sin\lambda ,$$

where λ is the angle between e_r'' and $\hat{P}$, and μ is the angle between e_1'' and the projection of $\hat{P}$ in the plane of e_1'' and e_2''. Furthermore, if θ_p and ϕ_p are the respective elevation and azimuth of $\hat{P}$, it follows that

$$\hat{P} = e_{\theta_c} \cos\theta_p \cos\phi_p + e_{\phi_c} \cos\theta_p \sin\phi_p + e_{r_c} \sin\theta_p . \tag{2.3}$$

We can also define P_1, P_2, P_3 - the vector components of $\hat{P}$ - by the transformation:

$$\begin{bmatrix} P_1 \\ P_2 \\ P_3 \end{bmatrix} = \begin{bmatrix} d_{11} & d_{12} & d_{13} \\ d_{21} & d_{22} & d_{23} \\ d_{31} & d_{32} & d_{33} \end{bmatrix} \begin{bmatrix} e_{\theta_c} \\ e_{\phi_c} \\ e_{r_c} \end{bmatrix} , \tag{2.4}$$

where each d_{ij} $(i,j=1,2,3)$ is a product of c_{ij} and the corresponding direction cosine of $\hat{P}$. Using the same technique as for e_r'', the coefficients of $e_{\theta_c}, e_{\phi_c}, e_{r_c}$ in (2.3) and (2.4) are equated, readily yielding θ_p and ϕ_p.

Finally, if V is any vector associated with the rocket flight, the angle between $\hat{P}$ and V may be derived. The unit vector in the direction of V is given by

$$\hat{V} = \frac{e_{\theta_c} v_1 + e_{\phi_c} v_2 + e_{r_c} v_3}{|V|} = e_{\theta_c} v_1' + e_{\phi_c} v_2' + e_{r_c} v_3' , \tag{2.5}$$

where the v_i (i=1,2,3) terms are the components of $\hat{V}$ in the directions of north, east and vertical; the resulting v_i' terms are thus the direction cosines of $\hat{V}$. The scalar product of (2.3) and (2.5) yields

$$\hat{P}\cdot\hat{V} = v_1' \cos\theta_p \cos\phi_p + v_2' \cos\theta_p \sin\phi_p + v_3' \sin\theta_p \quad .$$

Hence, the angle ψ, between $\hat{P}$ and $\hat{V}$ is given by:

$$\psi = \cos^{-1} (v_1' \cos\theta_p \cos\phi_p + v_2' \cos\theta_p \sin\phi_p + v_3' \sin\theta_p) \quad .$$

2.3 Data Refinement

Due to noise or in-flight calibrations often present in the recorded data, filtering procedures are modified or developed as required to provide continuous final output for the attitude determination system. The primary routines used are Fourier Series and n^{th} degree polynomial approximations.

To provide smooth, continuous and acceptable attitude information for vehicles when they have established angular precessional velocity and a half cone angle it is possible to generate gyro yaw and pitch information by means of the Fourier Series expansion. During this well-behaved areas of a particular vehicular flight, the coarse and/or fine yaw and pitch data can be predicted by the Fourier Series

$$y = \frac{a_o}{2} + \sum_{n=1}^{\infty} \left(a_n \cos \frac{n\pi x}{L} + b_n \sin \frac{\lambda\pi x}{L}\right) \quad .$$

This problem has proven successful due to the periodic nature of the data. However, for most rocket flights, quick convergence of the Fourier Series is obtained with the approximation

$$y = f_1 + f_2 t + f_3 \sin\omega t + f_4 \cos\omega t \quad .$$

The addition of the linear term is needed to account for an occasional linear shift in the converted data. A preliminary angular velocity ω is selected from a study of the oscillograms of the raw data, and is further refined by an option within the fitting routine.

During regions in which a vehicle is not coning, yaw and pitch outputs are separated into discrete time intervals. These intervals are then curve fitted with polynomials up to the 20^{th} degree when necessary. The n^{th} degree polynomial routine calculates an RMS value between measured and predicted data for each of the polynomial approximations. The minimum RMS value determines the degree of the polynomial approximation to be used in the specified interval.

The RMS is normally defined as

$$RMS = \sqrt{\sum_{i=1}^{N} \frac{(x_i - \bar{x})^2}{N}} \tag{2.6}$$

where x_i is the difference between a measured and predicted data value. To simplify computation and programming, an equivalent form of (2.6)

$$RMS = \sqrt{\sum_{i=1}^{N} \frac{x_i^2}{N} - \bar{x}^2} \tag{2.7}$$

was used. For a reasonably large sample size N, the RMS deviation approximates the standard deviation σ. Since a $\pm 3\sigma$ deviation accounts for $\approx$ 99.7% of the measured data in a normal distribution, tolerance levels are set on input data to ensure that all predicted data will be within the specified σ deviation while utilizing the results of (2.7).

Figures (8-22) show normal angles of attack using data refinement techniques.

SECTION 3

PHASE AND TIME SHIFT STUDIES

To corroborate the initial orientations of on-board sensors, measured and attitude predicted magnetometer pitch angles are compared. A software package was developed to compare the phase relationship during well-behaved areas of a vehicle's flight.

This package involves a least squares study on the magnetometer data (refer to Section 3.2 for a detailed description). The output produced includes a table of maximum (minimum) times T_{meas}, measured data values in degrees, associated ΔT_{meas} values and spin rates for the corrected magnetometer outputs. Also included are a table of maximum (minimum) times T_{gen}, predicted data values in degrees, associated ΔT_{gen} values and spin rates for the predicted magnetometer output from the attitude data. The two-time dependent tables are merged for all consecutive time values of each array and the phase shift between the associated values are printed.

For $T_{gen} \leq T_{meas} + \Delta T_{meas}$, the phase shift χ between the raw and the predicted magnetometer data is

$$\chi = \frac{T_{gen} - T_{meas}}{\Delta T_{meas}} \times 360^\circ$$

For $0 \leq \chi \leq 180^\circ$ the predicted data is lagging or coincident with the measured magnetometer data. For $180^\circ < \chi < 360^\circ$, the measured data is said to lag the predicted by $360^\circ - \chi$. The following figure depicts the relationships just discussed:

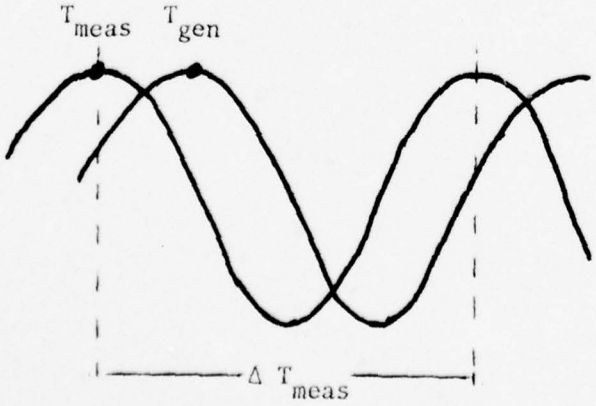

In the previous illustration, the predicted data from the attitude is lagging the raw data since we are assuming that $(T_{gen} - T_{meas}) \leq \frac{1}{2} \Delta T_{meas}$.

To check for possible timing problems, a time shift between measured and predicted data is computed. Statistical studies include a mean time shift and associated RMS value for each specified time interval.

3.1 Bias Equation

In order to accurately determine the times of maximum magnetometer output, smooth magnetometer readings are required. Normal data transmission does not provide such smooth output, so to allow for proper usage of the routines to be described in Section 3.2, a curve fit was put through the bias values of the magnetometer data. The samples selected are taken from the coning portion of flight - i.e., from approximately 40 kms. on ascent to approximately 40 kms. on descent.

Three equally spaced time intervals are selected to obtain a separate bias approximation B for each interval from the equation

$$B = \frac{\Sigma V_i}{n} .$$

A typical study will produce a value of n in the order of 2×10^4.

The standard bias equation as a function of time is normally approximated by a first degree polynomial. However to obtain greater aqcuracy with higher order terms in the fitting routine, the value of the bias B(t) as a function of

$$B(t) = at^2 + bt + c .$$

However, from the discussion above we can approximate B(t) by $\frac{\Sigma V_i}{n}$ in each of the intervals studied. This, in turn, leads to the system of equations

$$at_1^2 + bt_1 + c = B_1$$

$$at_2^2 + bt_2 + c = B_2$$

$$at_3^2 + bt_3 + c = B_3$$

where t_j, j=1,2,3 is taken as the mean time in the jth interval and

$$B_j = \frac{\sum_{i=1}^{n} V_i}{n} \qquad j=1,2,3$$

As the value of n increases, the maximum error that occurs in the approximation of B_j decreases. This fact can be verified by calculations on the on the expression $\frac{\Sigma V_i}{n}$.

This procedure to determine the bias equation as a function of time, forms part of the procedure used on all vehicle flights when examining phase shifts between measured and predicted data.

3.2 Maxima of the Magnetometer Measurements

Given the sinusoidal nature of the lateral magnetometer outputs, the prepared software routines have the capability of determining either the times of relative maximum outputs or the times of relative minimum outputs. If a least squares approximation of the data is desired in the maximum areas of the output, then a test is performed on the data V_i satisfying the inequality.

$$B(T_i) < V_i \ .$$

Likewise, if a fit of the minimum areas is desired, then only those V_i values satisfying the inequality

$$B(t_i) > V_i$$

are stored for computation in the least squares polynomial fits of the specified areas of the data.

In order to initiate the procedure for storing data in the maximum areas of the least squares approximation, a value V_i must be found such that $V_i > B(t_i)$ and $V_{i-1} \leq B(T_{i-1})$. Once initiated, data is stored until $V_i < B(t_j)$ and $V_{j-1} \geq B(t_{j-1})$ where $j > i$. This last condition is a necessary one for ending the sample region but not a sufficient condition. The sufficiency test is made by examining V_{j+1} to ensure that V_j is not a noise point. If $V_{j+1} < B(t_{j+1})$ then a least squares parabolic fit is performed on the sampled data. However, if $V_{j+1} \geq B(t_{j+1})$, the point V_j is discarded and the summing procedure of the least squares continues. Similar tests are made in the minimum regions of fitted data except that the inequality signs are reversed.

In each specified region, the data is fit to the quadratic

$$Y = \bar{A}t^2 + \bar{B}t + \bar{C} .$$

The value of the bias $B(t_i)$ at which the sampling begins and that value $B(t_j)$, $j > i$ at which the sampling ends are obviously just the points of inflection for the sinusoidal curve. The time of relative maximum (minimum) is obtained by setting $\frac{dY}{dt} = 0$ and solving for time t. This, in turn, provides us with a predicted output value

$$Y = \bar{A}T_M^2 + \bar{B}T_M + \bar{C}$$

where

$$T_M = -\frac{\bar{B}}{2\bar{A}} .$$

Should the measured and predicted outputs deviate by more than some specified limit, usually taken to be 4%, the acceptance level for least squares data may be modified so that the sampled regions more closely approximate the parabolic fit. This modification amounts to accepting the area containing maximum data when $V_i > B(t_i) + k$ where k is a constant determined from examination of the oscillographs. For minimum output regions, the inequality takes the form $V_i < B(t_i) - k$.

For each value of T_M generated by the 1st derivative test, an associated $Y(T_M)$ value and ΔT_M are output. Special note is made of any value of ΔT_M outside a specified interval about the assumed rotation rate and further investigations of these areas are undertaken as necessary. A mean ΔT_M value is computed for the well-behaved portion of the flight and output at the end of the data pass. This ΔT_M value for each lateral magnetometer normally consists of spin and precessional motion and, therefore, is referred to as the rotation rate.

Although no specific mention as yet has been made of the axial magnetometer output, the routines apply equally as well in the case of this magnetometer. Computation of maximum and minimum values provide us with a good approximation to the cone angle of the vehicle axis. Should the output exhibit only the slightest variance in successive maximum and minimum values respectively, then the vehicle axis motion is due almost entirely to precessional motion and the cone angle will remain nearly constant.

If the vehicle axis study option is desired in addition to the lateral magnetometers, supplemental outputs include the cone angles and precessional period of the vehicle axis. Examples of normal outputs are displayed in Figures 23 A & B.

SECTION 4

CORRECTION PROCEDURES FOR ROCKETS WHOSE GYRO SYSTEMS MALFUNCTION

Some of the more common types of problems with gyro systems include situations in which the gyro's roll output remain constant for a portion of a spin or the gyro measurements go outside its calibrated limits either with or without loss of initial reference. Examples of such problems and correction techniques follow.

The vehicles A09.303-4 and A10.312-3 had onboard MIDAS gyro systems whose gyro roll output remained constant for a portion of a spin (Fig. 24). To correct th problem, a roll rate was established for the ill defined flight areas. These roll rates were calculated from the roll data on each spin that was not influenced by this malfunction, and they were substantiated by rotation rates determined from the measurements of a magnetometer which was mounted normal to the rocket axis. Utilizing the predicted vehicle roll rate, a lock was made on the well defined area and continuous roll output resulted.

The ACS system for the vehicle IC630.02-1A went outside its calibrated limits (Fig. 25) on the pitch axis but never lost its initial reference from the point of uncaging. Converted reliable true pitch (P_T) data as a function of time was available for various P_T values in which

$$0^\circ \leq P_T \leq 110^\circ$$

$$250^\circ \leq P_T \leq 358^\circ \quad .$$

These reliable data points were used as samples for least squares polynomial fits (see Section 2.3) in each of the various time intervals during which saturation occurred. The criterion for an acceptable polynomial approximation was not only a minimum and acceptable RMS value between predicted and non-saturated measure P_T values, but also continuity between the predicted P_T data in the saturation areas and measured P_T data in the non-saturated areas.

Recovery procedures for vehicle IC511.21-1A were much more involved than those discussed above. The oscillogram inspection indicated that the gyro malfunctioned from 250-305 seconds. To predict yaw data in this interval, an in-depth analysis and examination of the plots of gyro measurements suggested a modified Fourier Series of the form

$$A + Bt + C \sin\omega t + D \cos\omega t$$

be used. Examination of the raw data showed an acceptable precessional period to be 11.2984 seconds and accordingly we set the angular velocity

$$\omega = \frac{2\pi}{112.984} \ .$$

Results of computer runs produced a yaw RMS of 0.6°. This was deemed acceptable and the equation to fit yaw data in degrees as a function of time t was defined as

$$\text{Yaw}(\overline{T}) = A + B\overline{T} + C \sin\omega\overline{T} + D \cos\omega\overline{T}$$

where

$$\overline{T} = t-100 \text{ and } 250 \leq t \leq 308$$

$$A = -14.234 \qquad B = -.006 \qquad C = -6.354 \qquad D = -15.838$$

and ω is as described above.

To predict pitch data in the above mentioned interval, plots suggested a polynomial approximation be used due to the relative steepness of slope in available pitch output. A thorough examination of plots indicated that a structure in the pitch data from 250-308 seconds was similar to measurements in the portion from 130-198 seconds after launch. A cubic equation yielding an RMS value of .5159° produced the best polynomial approximation to the pitch data in this well-behaved area.

By the Weierstrass approximation theorem (Reference [2], page 102), we introduced the function

$$\Delta y = \frac{1}{28}(t-271.9) \qquad t\varepsilon[250,308]$$

and predicted pitch data in the closed interval $250 \leq t \leq 308$ by the equation

$$\text{Pitch}(t) = A\overline{T}^3 + B\overline{T}^2 + C\overline{T} + D\,\Delta y \ , \quad \overline{T} = t-213 \ .$$

The constants in the Δy function were determined by the available pitch data. The values of coefficients determined by a linear least squares estimation (Reference [1]) were found to be

$$A = -.0003433064 \qquad B = .06455981 \qquad C = -3.135508 \qquad D = -1.314757 .$$

Substituting the values of the coefficients and replacing $\overline{T}$ by t-213, the equation to predict angular pitch data becomes

$$\text{Pitch}(t) = -.0003433064t^3 + .2839306826t^2 - 77.32826863tt - 6903.397458$$

with an RMS value of .5980°.

From the Roll Rate program, the vehicle's roll rate was established for this gapped area and through continuity checks was locked into the roll data. All gyro corrections were incorporated into the aspect program to provide continuous preliminary attitude for the entire flight.

Furthermore, a phase shift study between the actual magnetometer measurements and those simulated using attitude information was initiated. The results of this study showed an average time shift between maximum predicted and maximum measured magnetometer attack angles to be .0554 seconds with an RMS of .0048 seconds for the interval from launch to 54 seconds in flight. A similar time shift study from 107 to 272 seconds showed the average time shift between maximum attack angles to be .1694 seconds with an RMS of .0182 seconds. Phase shift displacement angles were also generated throughout the vehicle lifetime, but they did not show a constant shift. The spin rate change varied from .6 rps to 4.1 rps from launch to 107 seconds and then stabilized at 1.08 rps.

In an attempt to use the times of the maximums and minimums of the actual magnetometer measurements to further refine the roll data, an analysis was developed using the yaw and pitch data at the times of the above mentioned magnetometer measurements, the orientation of the magnetometer and the gyro reference notch. To implement this analysis, the yaw and pitch data was merged with the times of maximums and minimums of the actual magnetometer data as supplied by the detailed phase study.

A software routine was then prepared to calculate the discrete gyro roll using the merged gyro information and theoretical model of the Earth's magnetic field. The results of this program were studied and continuous roll was generated for this flight using these calculated discrete roll values.

In the judgement of the Initiator of this problem, it was decided that the roll data calculated using the refinement technique of incorporating phase shift outputs compared most favorably with his attitude sensitive experimental results.

Figures (26-28)display the final angles of attack of these vehicles using the various mentioned correction procedures.

Figure 8

BEST AVAILABLE COPY

BEST AVAILABLE COPY

Figure 9

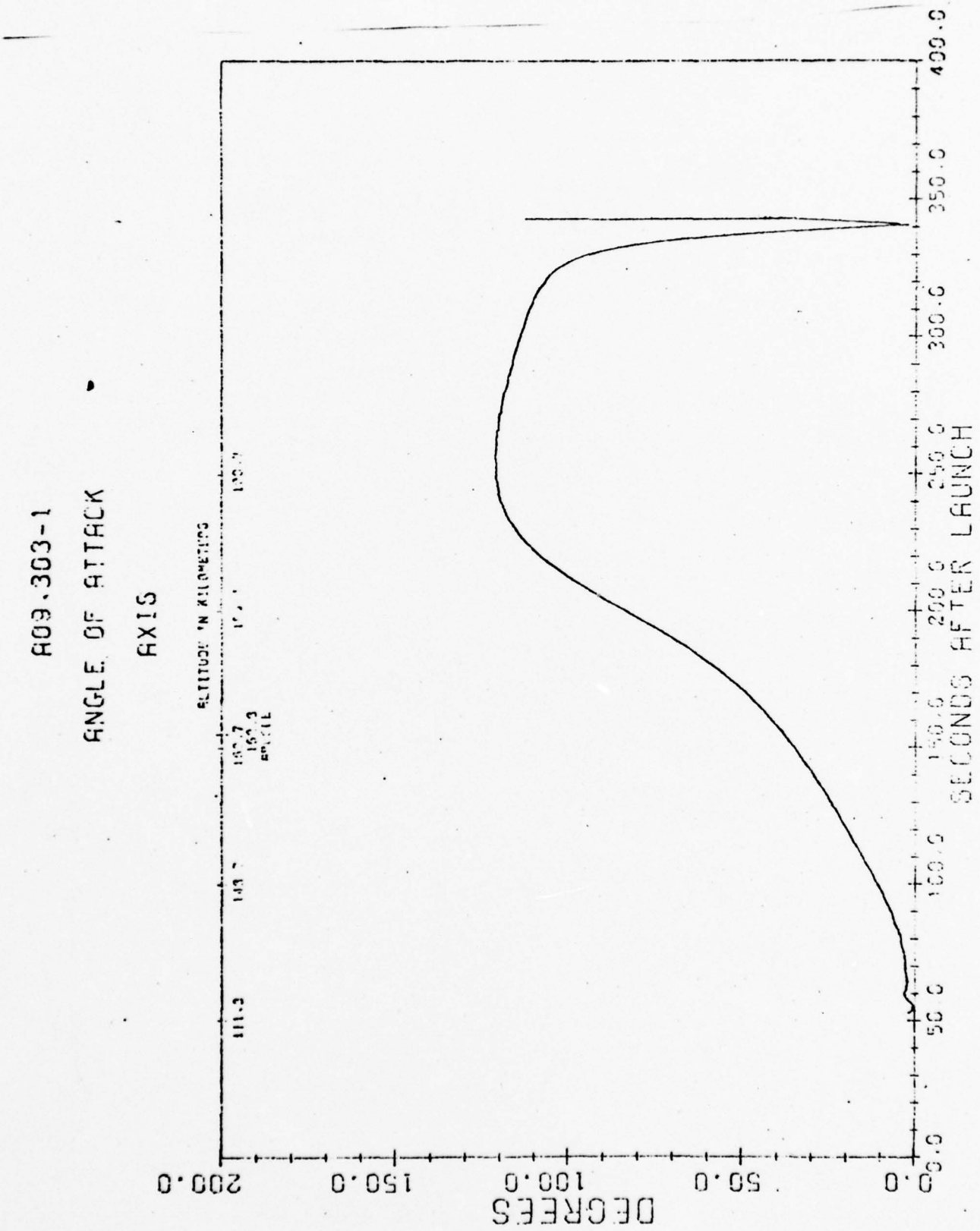

Figure 10

BEST AVAILABLE COPY

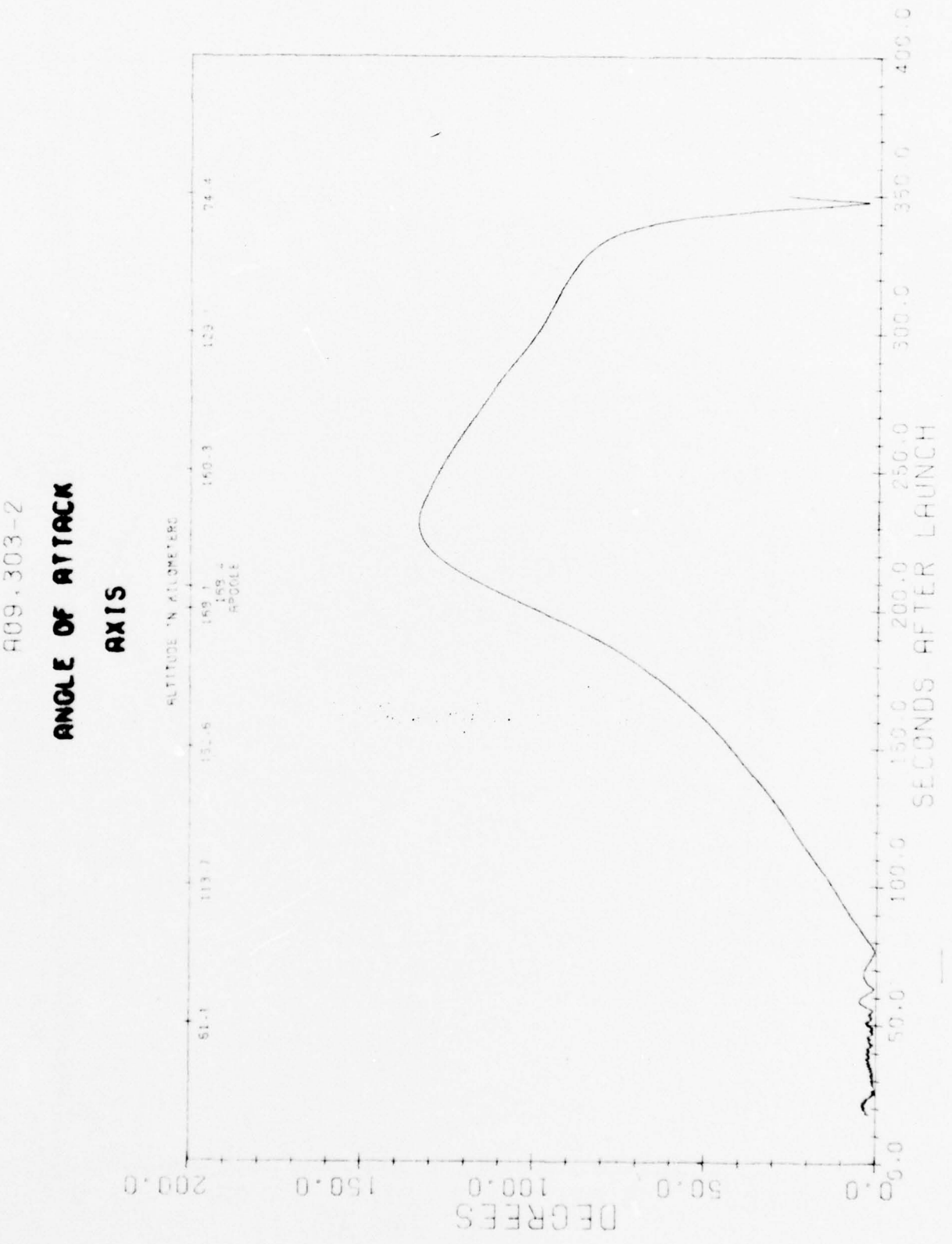

Figure 11

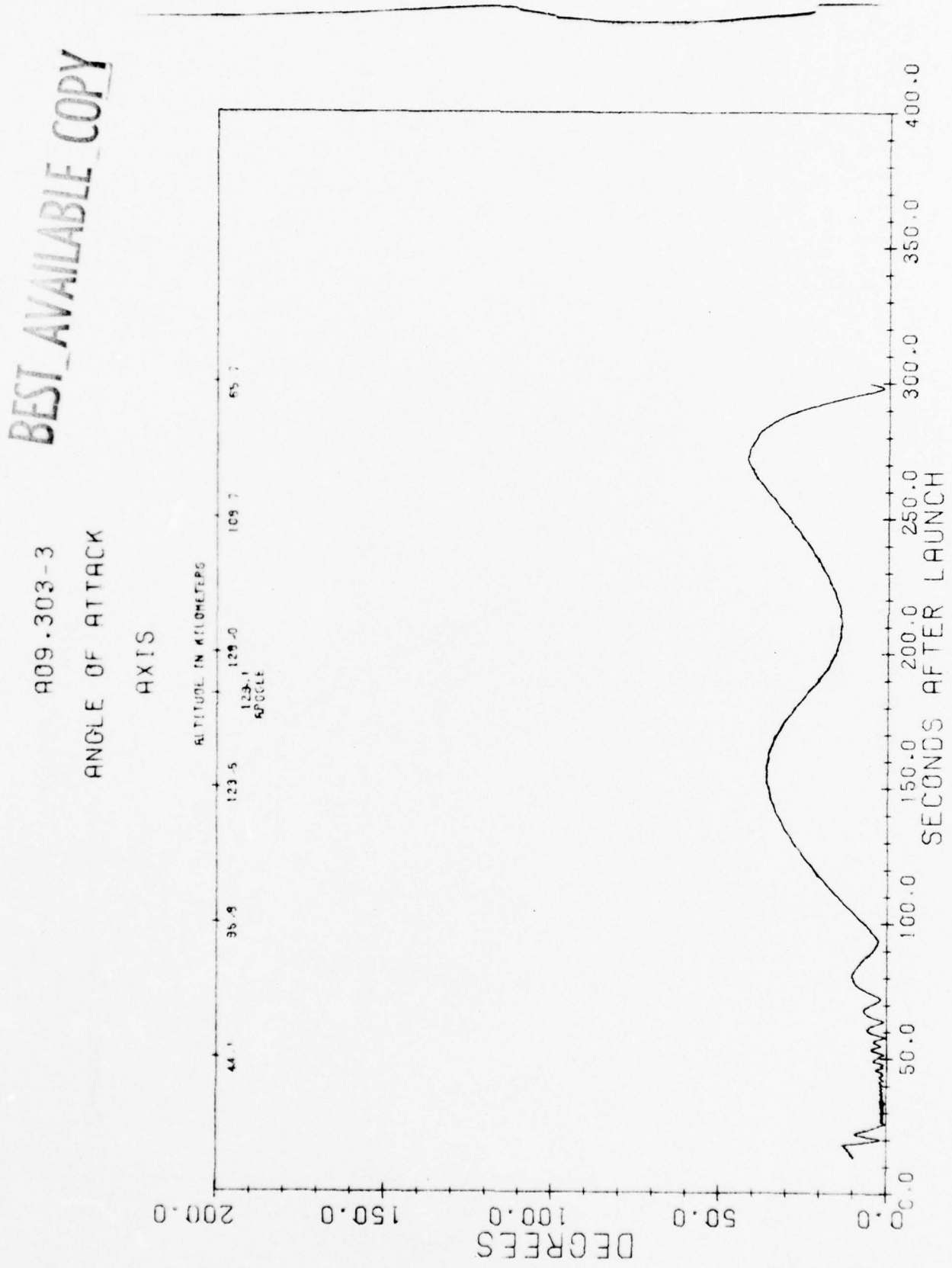
BEST AVAILABLE COPY
A09-303-3
ANGLE OF ATTACK
AXIS
ALTITUDE IN KILOMETERS
123.5
129.0
109.7
95.9
44.1
DEGREES
0.0
50.0
100.0
150.0
200.0
SECONDS AFTER LAUNCH
0.0
50.0
100.0
150.0
200.0
250.0
300.0
350.0
400.0

Figure 12

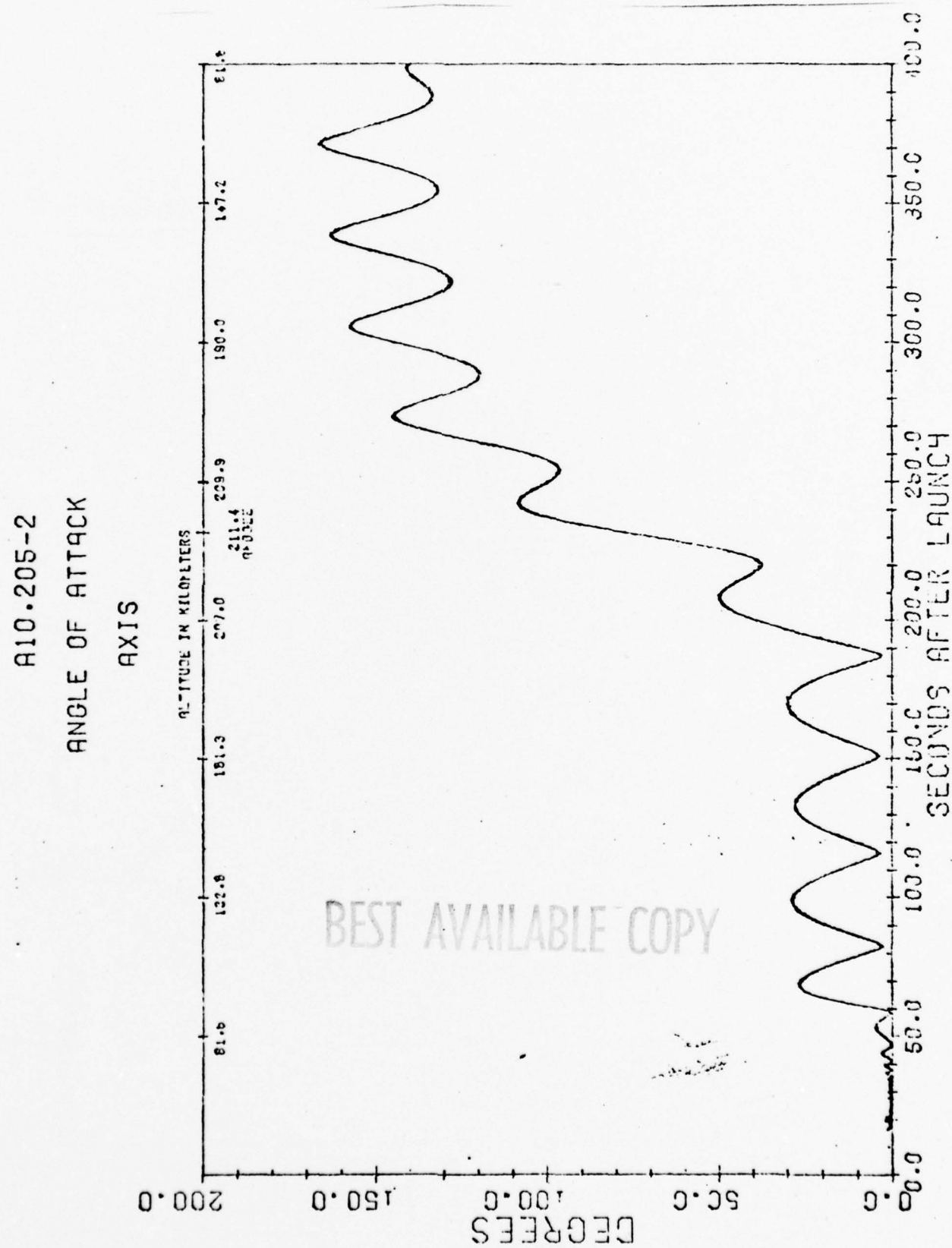

BEST AVAILABLE COPY

Figure 13


BEST AVAILABLE COPY
A10-213-1
ANGLE OF ATTACK
AXIS
ALTITUDE IN KILOMETERS
DEGREES
SECONDS AFTER LAUNCH
0.0
50.0
100.0
150.0
200.0
250.0
300.0
350.0
400.0

Figure 14

BEST AVAILABLE COPY

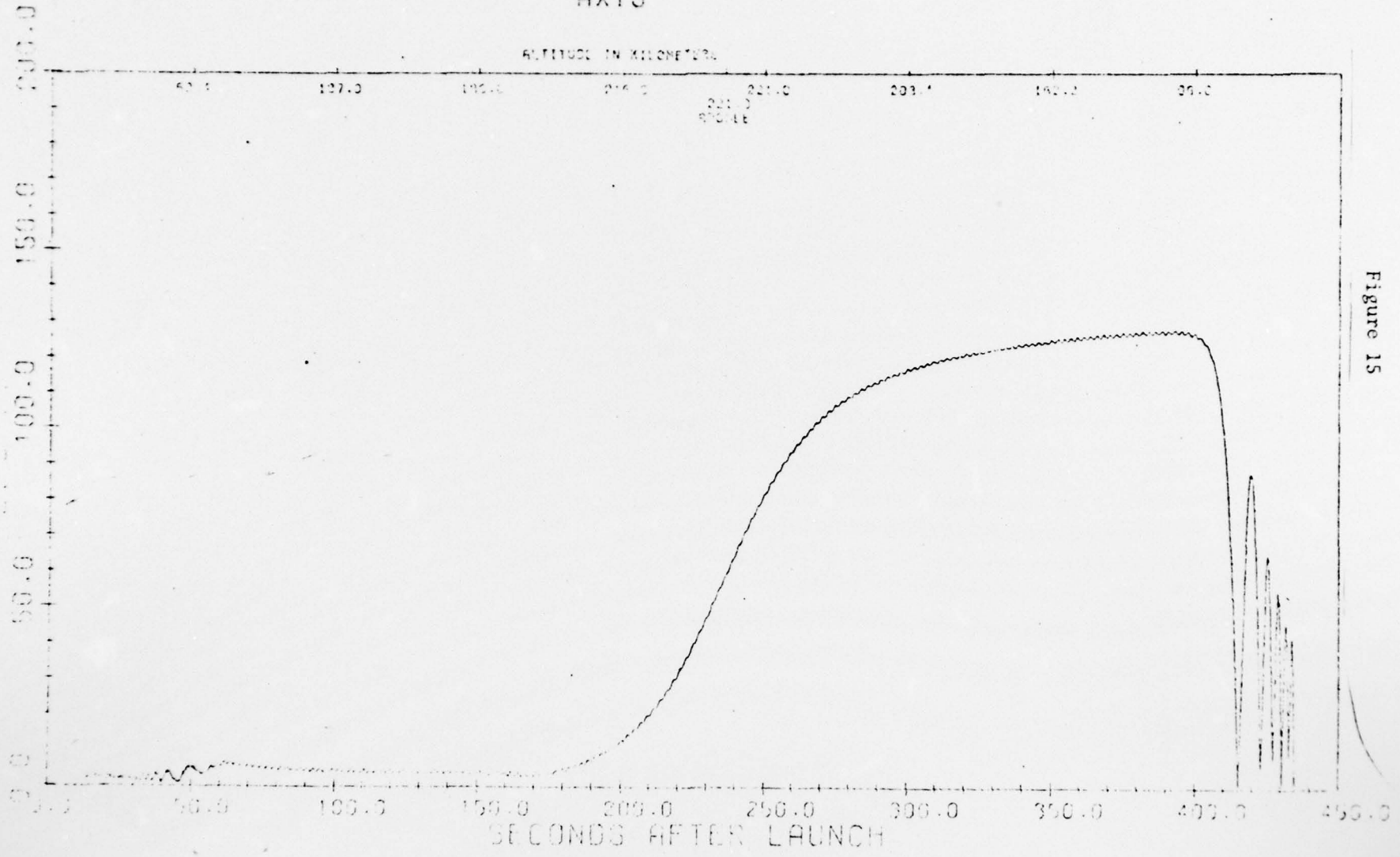

Figure 15

Figure 16

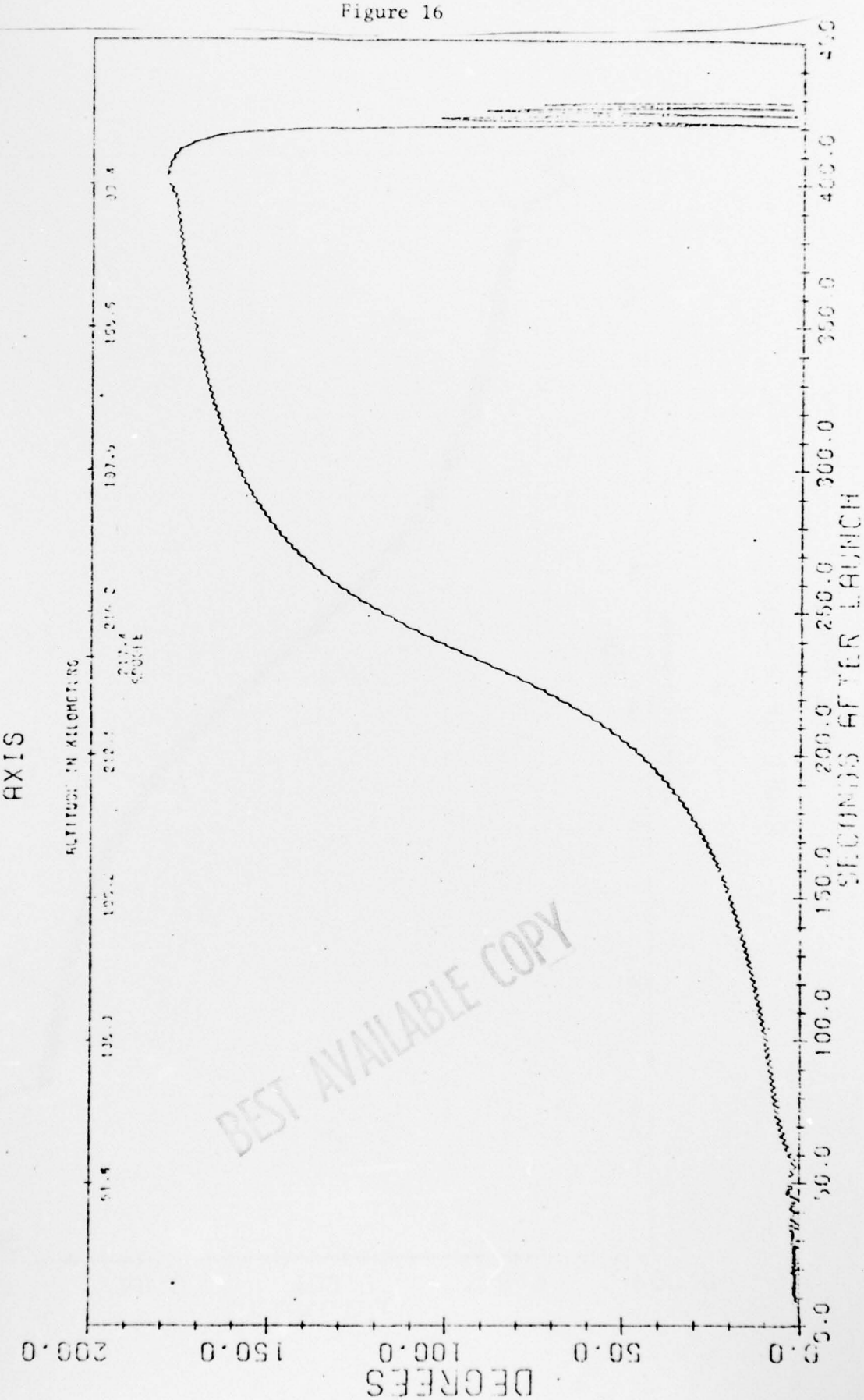

BEST AVAILABLE COPY

Figure 17

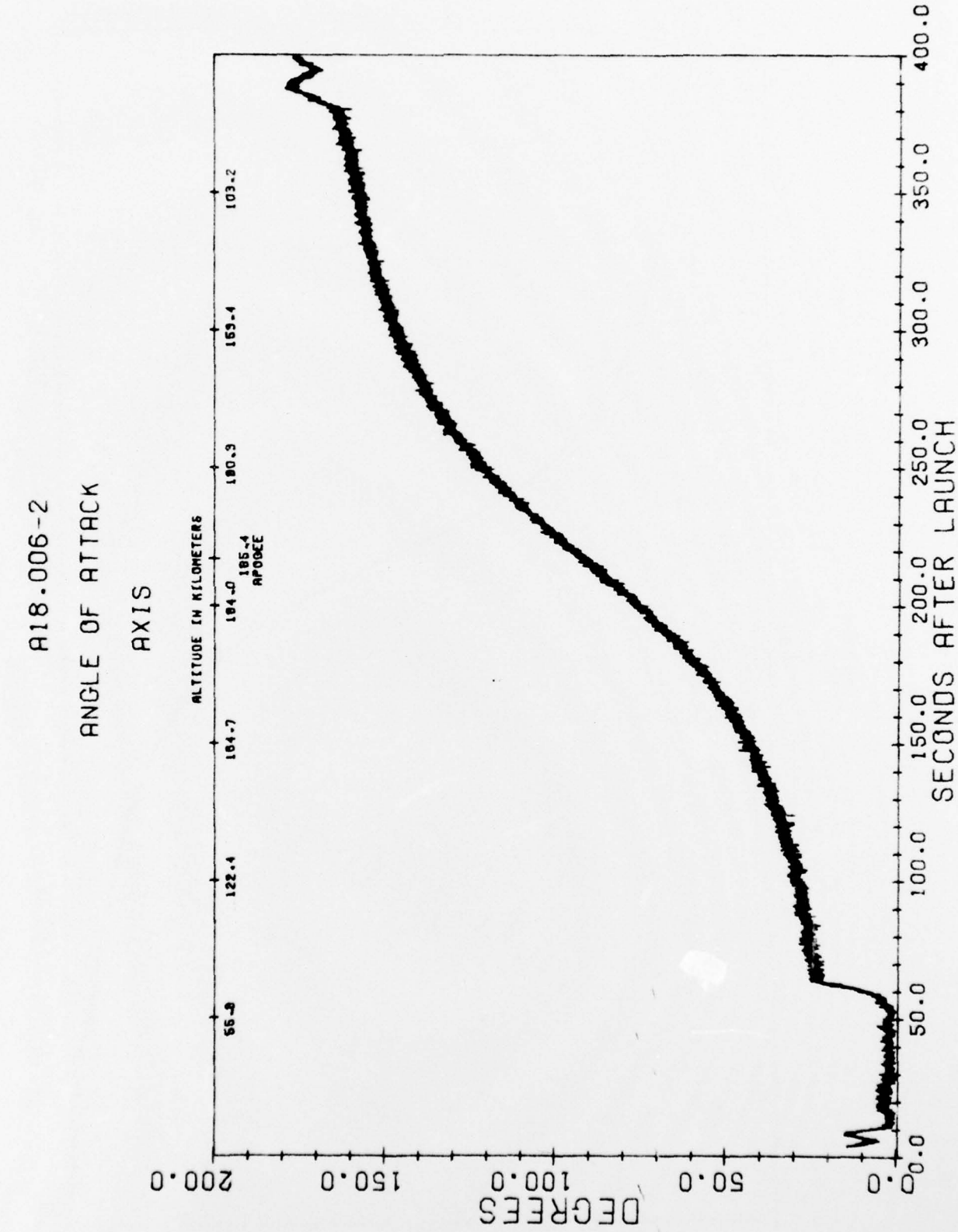
A18.006-2
ANGLE OF ATTACK
AXIS
ALTITUDE IN KILOMETERS
55.9
122.4
164.7
184.0
185.4
APOGEE
180.3
169.4
103.2
0.0
50.0
100.0
150.0
200.0
250.0
300.0
350.0
400.0
SECONDS AFTER LAUNCH
0.0
50.0
100.0
150.0
200.0
DEGREES

Figure 18

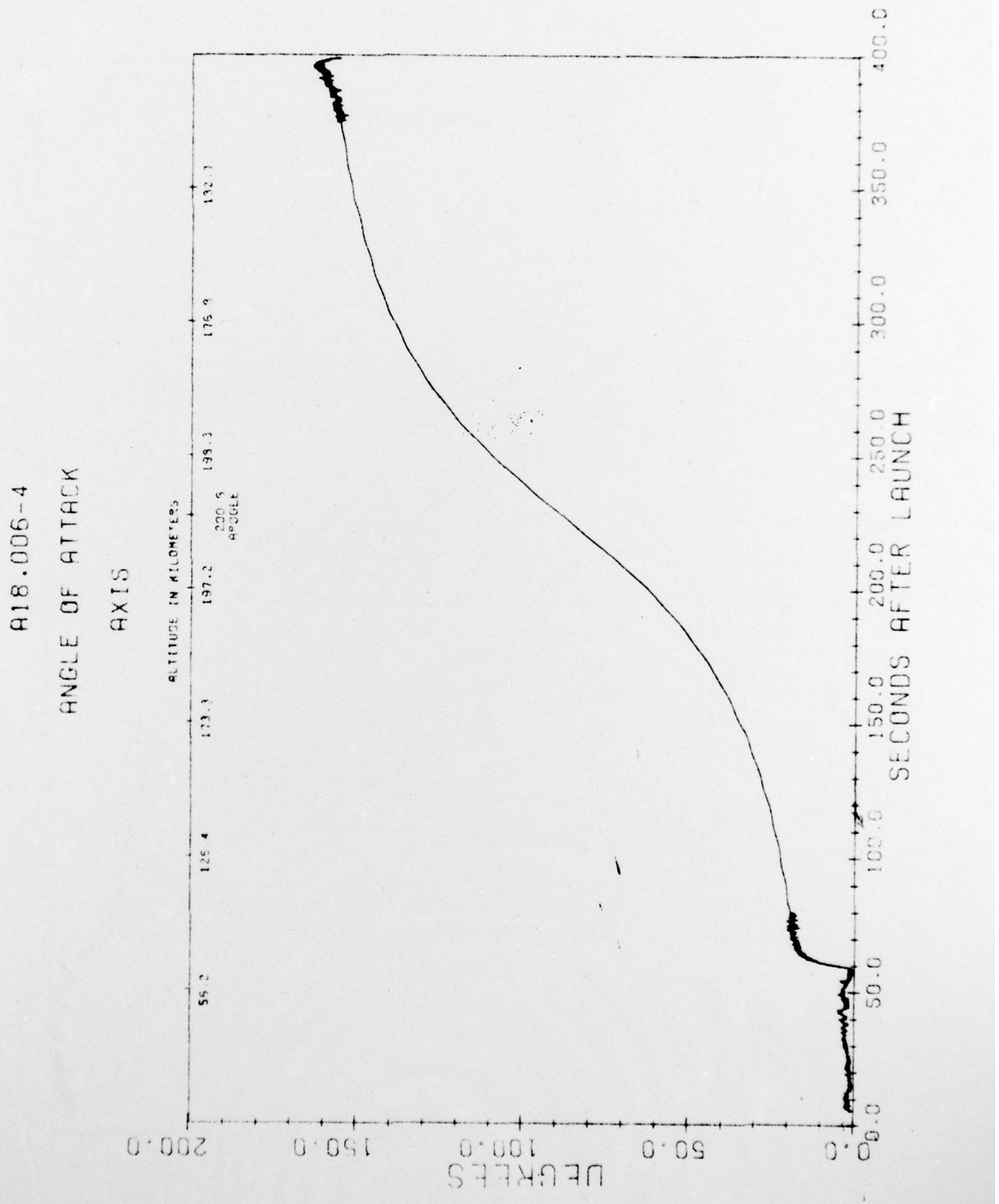
A18.006-4
ANGLE OF ATTACK
AXIS
ALTITUDE IN KILOMETERS
55.2
125.4
133.3
197.2
200.5
APOGEE
199.3
175.9
132.1
DEGREES
0.0
50.0
100.0
150.0
200.0
SECONDS AFTER LAUNCH
0.0
50.0
100.0
150.0
200.0
250.0
300.0
350.0
400.0

Figure 19

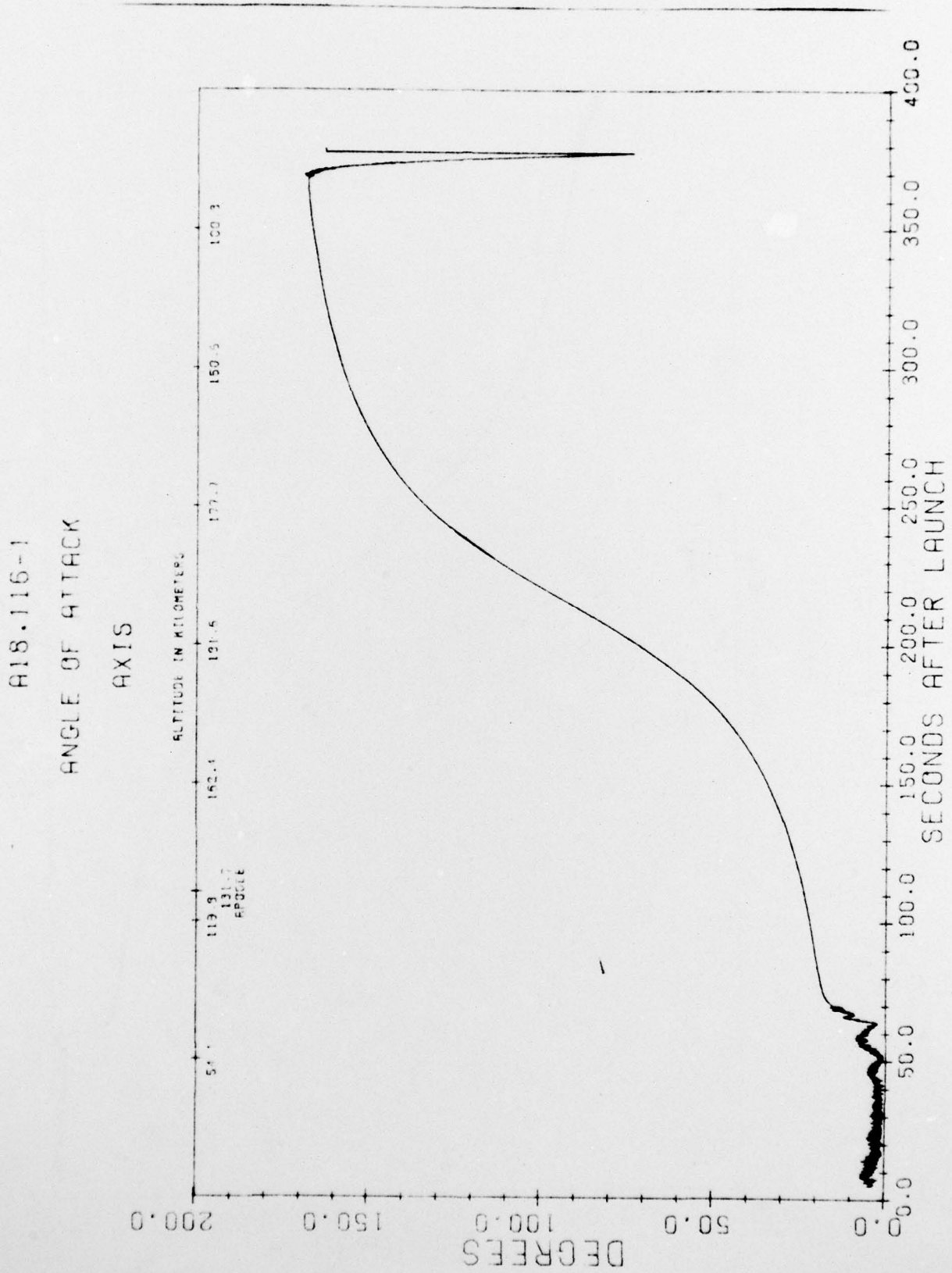
A18.116-1
ANGLE OF ATTACK
AXIS
ALTITUDE IN KILOMETERS
DEGREES
SECONDS AFTER LAUNCH
0.0
50.0
100.0
150.0
200.0
250.0
300.0
350.0
400.0

Figure 20

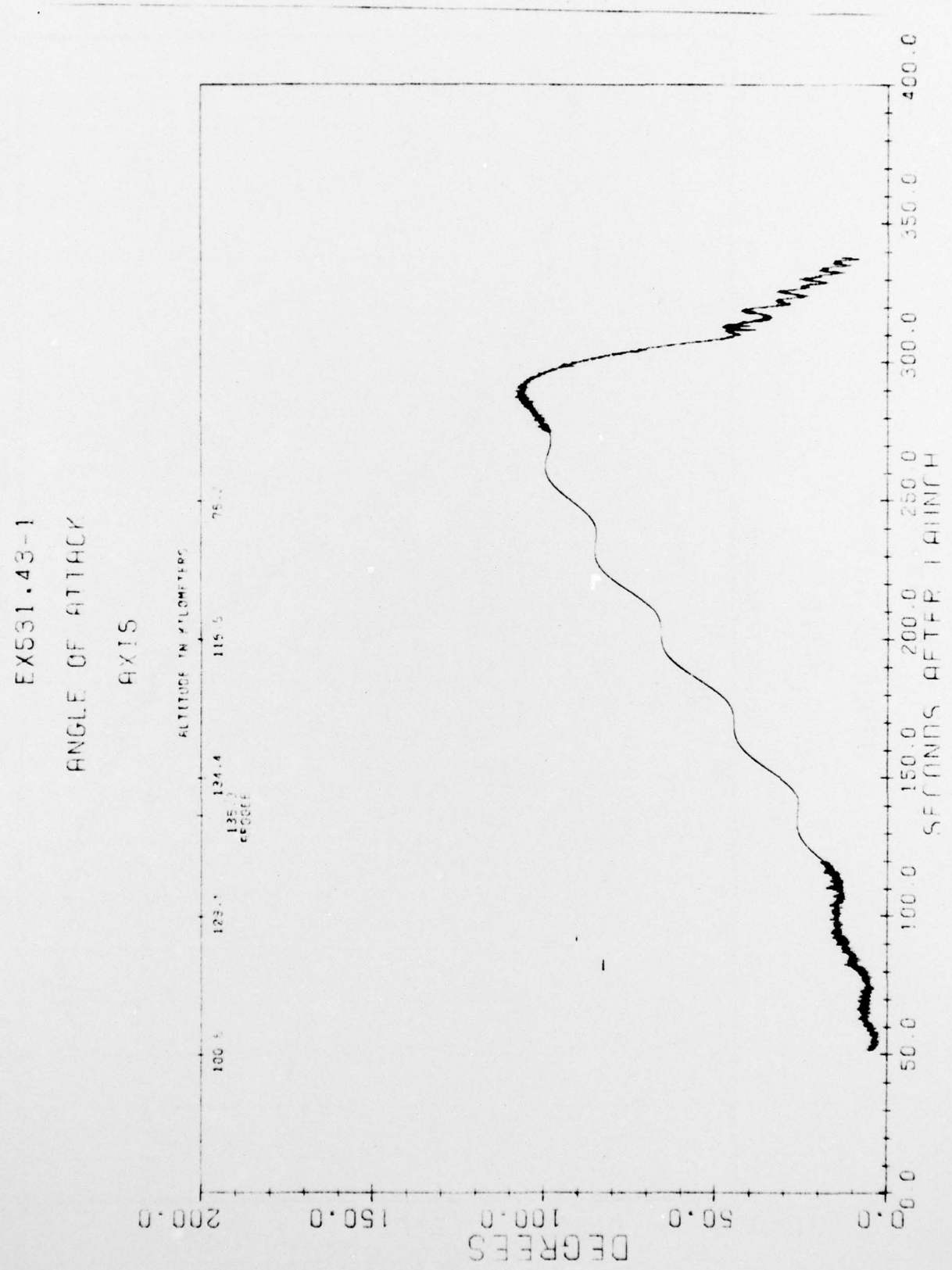
EXS31.43-1
ANGLE OF ATTACK
AXIS
DEGREES
0.0
50.0
100.0
150.0
200.0
SECONDS AFTER LAUNCH
0.0
50.0
100.0
150.0
200.0
250.0
300.0
350.0
400.0

Figure 21

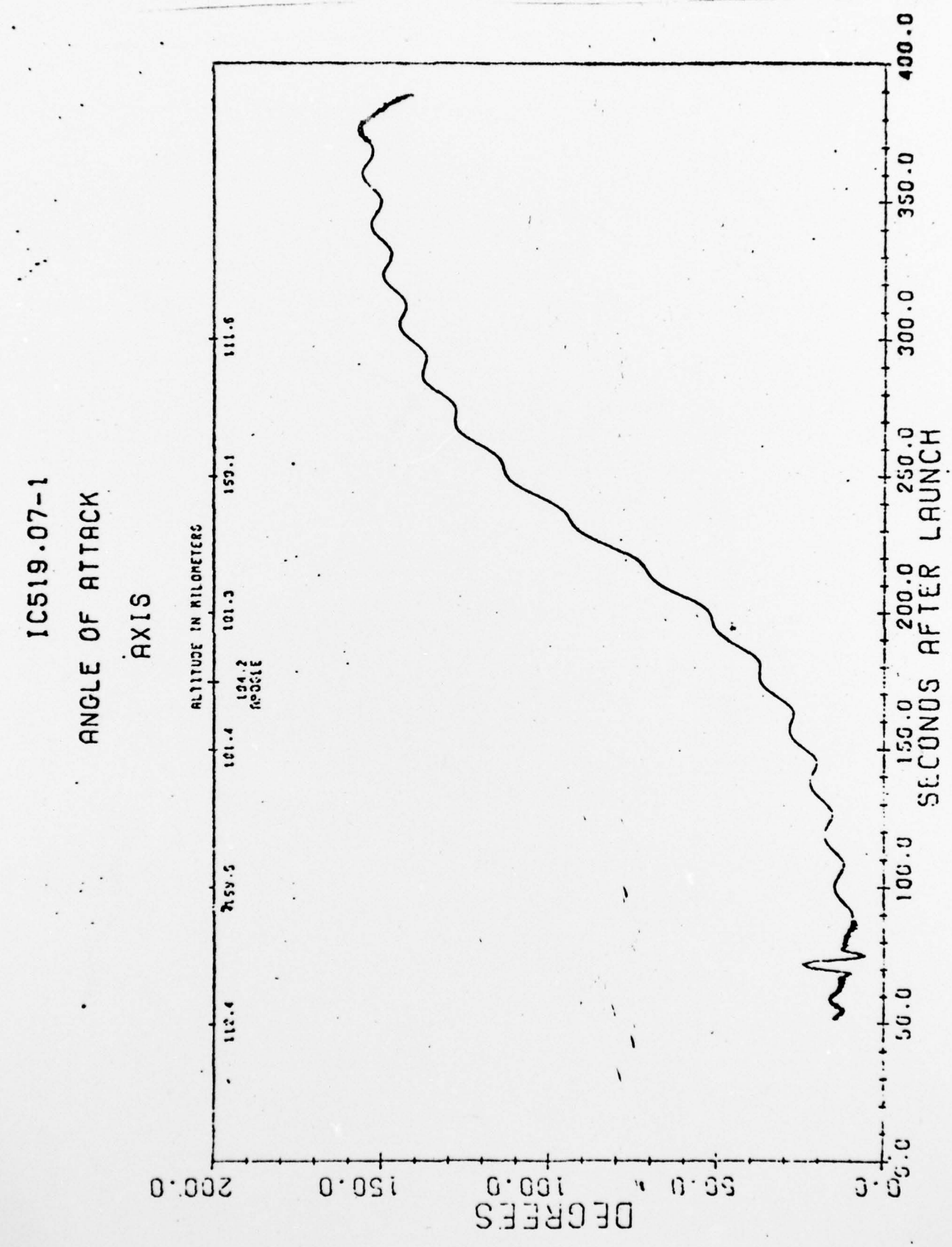
IC519.07-1
ANGLE OF ATTACK
AXIS
ALTITUDE IN KILOMETERS
111.6
159.1
101.3
101.4
124.2
ROCKET
DEGREES
200.0
150.0
100.0
50.0
0.0
0.0
50.0
100.0
150.0
200.0
250.0
300.0
350.0
400.0
SECONDS AFTER LAUNCH

Figure 22

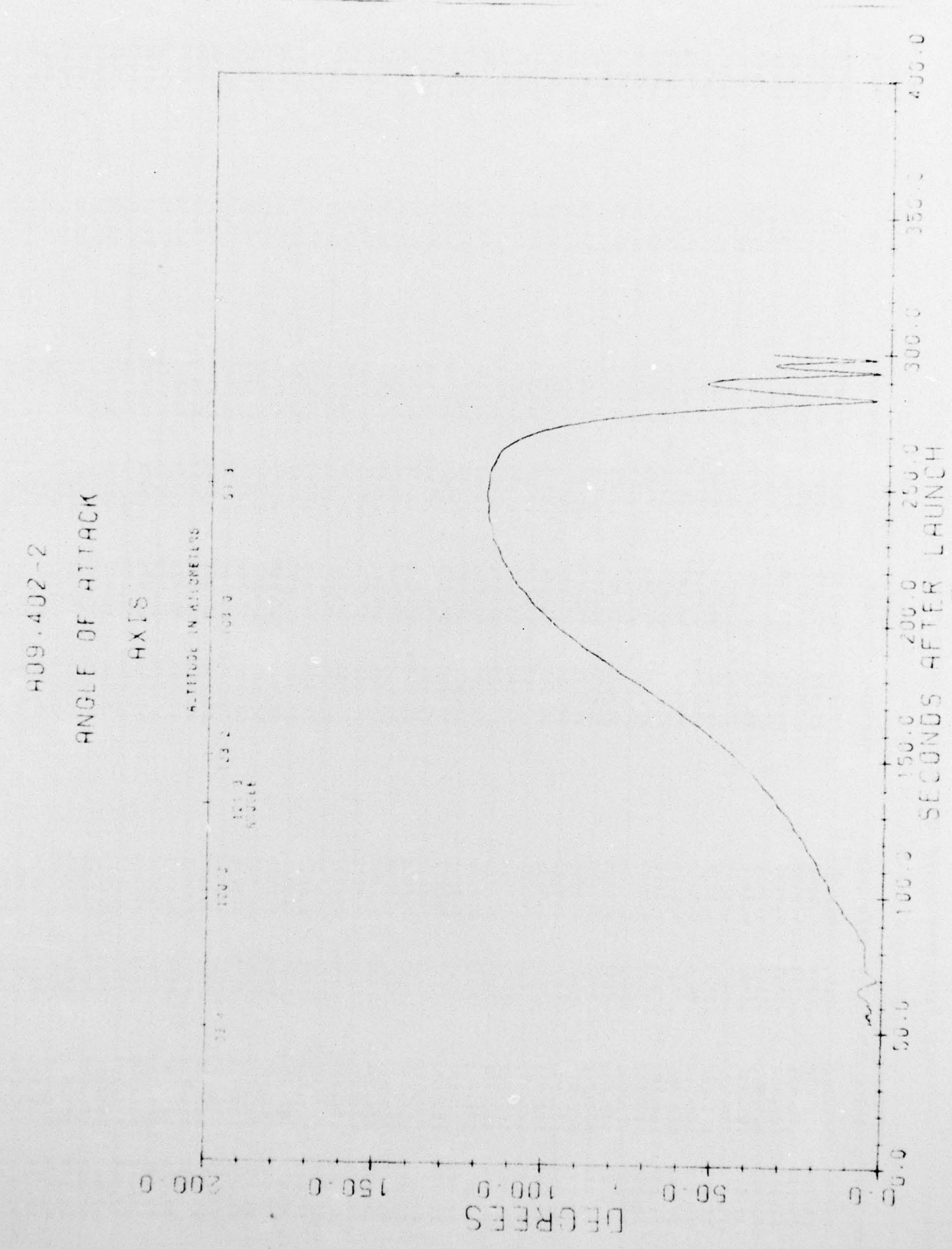
A09.402-2
ANGLE OF ATTACK
AXIS
DEGREES
SECONDS AFTER LAUNCH
0.0
50.0
100.0
150.0
200.0
250.0
300.0
350.0
400.0

PHASE SHIFT BETWEEN THE MEASURED AND GENERATED MAGNETOMETER OUTPUTS

GENERATED OUTPUT				MEASURED OUTPUT				PHASE	TIME
MAX TIME	ANGLE	DELTAT	SPIN RATE	MAX TIME	ANGLE	DELTAT	SPIN RATE	SHIFT	SHIFT
29.507	100.717	.2154	4.6425	29.553	96.453	.2180	4.5872	76.21	.0456
29.751	100.423	.2235	4.4743	29.776	96.887	.2229	4.4863	72.48	.0450
29.954	100.905	.2239	4.4663	29.999	96.674	.2235	4.4743	71.87	.0447
30.181	100.962	.2265	4.4150	30.226	96.216	.2269	4.4072	71.68	.0451
30.413	100.922	.2325	4.3011	30.460	96.337	.2342	4.2699	72.46	.0468
30.642	101.117	.2282	4.3821	30.686	96.427	.2280	4.3860	73.67	.0467
30.884	100.472	.2407	4.1545	30.930	96.338	.2414	4.1425	70.89	.0474
31.115	101.628	.2329	4.2937	31.161	96.537	.2317	4.3153	71.26	.0461
31.357	100.648	.2406	4.1391	31.400	97.041	.2387	4.1894	64.22	.0431
31.600	100.921	.2432	4.1118	31.647	96.133	.2472	4.0453	70.02	.0473
31.837	101.309	.2379	4.2105	31.885	97.210	.2375	4.2105	71.70	.0473
32.089	100.313	.2512	3.9809	32.132	96.084	.2475	4.0406	62.34	.0435
32.332	101.626	.2417	4.1034	32.379	97.802	.2466	4.0552	68.94	.0464
32.582	100.836	.2492	4.0128	32.629	97.105	.2504	3.9935	68.76	.0476
32.817	100.775	.2553	3.9170	32.883	96.201	.2533	3.9479	64.44	.0457
33.065	101.675	.2487	4.0209	33.133	97.515	.2508	3.9872	69.34	.0479
33.342	100.799	.2564	3.9002	33.389	96.836	.2552	3.9185	65.57	.0467
33.602	100.851	.2598	3.8491	33.644	96.626	.2558	3.9093	59.17	.0427
33.855	101.658	.2547	3.9268	33.903	97.721	.2583	3.8715	65.44	.0463
34.117	101.312	.2602	3.8432	34.162	96.913	.2593	3.8565	62.81	.0454
34.382	100.566	.2650	3.7736	34.429	96.474	.2673	3.7411	64.80	.0477
34.641	101.315	.2596	3.8521	34.686	97.295	.2567	3.8955	62.13	.0448
34.901	101.597	.2601	3.8447	34.947	97.382	.2615	3.8241	63.94	.0462
35.170	100.802	.2687	3.7216	35.216	96.785	.2689	3.7189	62.17	.0464
35.435	100.568	.2653	3.7693	35.481	96.607	.2642	3.7858	61.47	.0453
35.693	101.590	.2635	3.7951	35.746	97.629	.2652	3.7707	64.08	.0469
35.957	101.450	.2685	3.7244	36.013	97.532	.2674	3.7397	61.41	.0458
36.237	100.594	.2700	3.7037	36.284	96.601	.2708	3.6923	62.27	.0467
36.506	100.830	.2690	3.7175	36.551	97.024	.2674	3.7397	60.35	.0451
36.774	101.685	.2679	3.7327	36.821	97.432	.2699	3.7051	63.23	.0471
37.045	100.830	.2721	3.6751	37.091	97.291	.2698	3.7064	59.27	.0448
37.322	100.775	.2761	3.6219	37.368	97.131	.2773	3.6062	59.98	.0460
37.594	101.314	.2717	3.6805	37.639	96.653	.2711	3.6887	60.15	.0454
37.863	101.459	.2638	3.7202	37.909	97.555	.2698	3.7064	62.14	.0464
38.136	101.255	.2736	3.6550	38.182	97.187	.2732	3.6603	60.53	.0460
38.414	100.549	.2775	3.6036	38.463	97.384	.2811	3.5702	63.05	.0486
38.691	101.099	.2766	3.6153	38.736	96.914	.2737	3.6536	59.48	.0457
38.953	101.424	.2727	3.6670	39.011	97.857	.2750	3.6364	63.37	.0480
39.235	101.869	.2720	3.6765	39.282	97.508	.2712	3.6873	62.47	.0472
39.511	101.291	.2757	3.6271	39.558	96.776	.2757	3.6271	61.63	.0472
39.791	100.886	.2798	3.5746	39.835	96.783	.2759	3.6114	57.00	.0443
40.070	101.149	.2793	3.5804	40.115	96.675	.2801	3.5702	58.13	.0451
40.346	101.799	.2762	3.6206	40.394	98.129	.2787	3.5881	62.04	.0476
40.619	102.021	.2731	3.6617	40.666	98.602	.2720	3.6765	61.30	.0465
40.897	101.648	.2779	3.5984	40.941	97.845	.2754	3.6311	57.00	.0440
41.178	100.964	.2804	3.5663	41.222	97.666	.2806	3.5638	56.75	.0442
41.458	100.400	.2884	3.5663	41.501	96.724	.2790	3.5842	55.08	.0429
41.739	100.955	.2800	3.5714	41.784	97.030	.2832	3.5311	59.27	.0461
42.016	101.706	.2742	3.5945	42.062	97.258	.2783	3.5932	59.65	.0461
42.234	102.245	.2782	3.5945	42.339	97.910	.2765	3.6165	57.71	.0446

Figure 23A

PHASE SHIFT BETWEEN THE MEASURED AND GENERATED MAGNETOMETER OUTPUTS

GENERATED OUTPUT				MEASURED OUTPUT				PHASE	TIME
MAX TIME	ANGLE	DELTAT	SPIN RATE	MAX TIME	ANGLE	DELTAT	SPIN RATE	SHIFT	SHIFT
179.611	136.169	.9779	1.0226	178.726	127.704	.9763	1.0243	15.92	.0457
173.661	136.839	.9811	1.0203	179.708	127.619	.9815	1.0183	17.30	.0471
180.638	137.533	.9776	1.0229	180.684	128.487	.9765	1.0241	17.81	.0462
181.617	137.985	.9790	1.0215	181.665	128.783	.9807	1.0197	17.61	.0479
182.597	138.920	.9800	1.0204	182.644	129.983	.9784	1.0221	17.01	.0463
183.575	139.443	.9785	1.0220	183.623	129.853	.9797	1.0207	17.51	.0476
184.556	139.844	.9800	1.0204	184.602	130.660	.9792	1.0212	17.15	.0467
185.536	140.811	.9803	1.0201	185.584	130.771	.9817	1.0186	17.70	.0482
186.515	141.300	.9792	1.0212	186.562	131.203	.9775	1.0230	17.10	.0465
187.497	141.728	.9819	1.0184	187.545	132.261	.9835	1.0168	17.64	.0481
188.477	142.460	.9801	1.0203	188.524	132.106	.9785	1.0222	17.99	.0469
189.458	143.364	.9810	1.0194	189.506	133.135	.9823	1.0180	17.50	.0477
190.441	143.680	.9827	1.0176	190.488	133.172	.9823	1.0180	17.33	.0473
191.422	144.434	.9819	1.0184	191.469	134.009	.9804	1.0200	17.14	.0467
192.414	145.131	.9821	1.0182	192.458	134.283	.9843	1.0160	17.95	.0490
193.388	145.754	.9836	1.0167	193.435	135.123	.9822	1.0181	17.42	.0476
194.370	146.332	.9820	1.0183	194.418	135.384	.9828	1.0175	17.74	.0484
195.354	147.121	.9840	1.0163	195.401	135.954	.9830	1.0173	17.34	.0474
196.339	147.679	.9842	1.0161	196.387	135.982	.9858	1.0142	17.95	.0491
197.322	148.226	.9843	1.0160	197.369	136.552	.9826	1.0177	17.37	.0475
198.308	148.948	.9859	1.0143	198.357	137.587	.9877	1.0125	15.84	.0494
199.293	149.634	.9856	1.0146	199.340	137.356	.9833	1.0170	17.17	.0470
200.279	150.307	.9858	1.0144	200.327	138.189	.9870	1.0132	17.63	.0482
201.267	151.011	.9876	1.0126	201.316	138.501	.9885	1.0115	17.90	.0491
202.254	151.726	.9875	1.0127	202.302	139.573	.9861	1.0141	17.33	.0477
203.243	152.385	.9884	1.0117	203.291	139.602	.9890	1.0111	17.56	.0482
204.232	153.268	.9896	1.0105	204.280	140.293	.9886	1.0115	17.21	.0473
205.222	154.046	.9899	1.0102	205.272	141.027	.9920	1.0081	17.97	.0494
206.213	154.647	.9908	1.0093	206.261	141.265	.9897	1.0104	17.59	.0484
207.215	155.467	.9926	1.0075	207.255	141.887	.9938	1.0062	19.03	.0497
208.195	156.706	.9927	1.0074	208.248	142.241	.9923	1.0078	17.89	.0493

THE AVERAGE TIME SHIFT IS .0475 WITH AN RMS OF .0024

Figure 23B

Figure 24

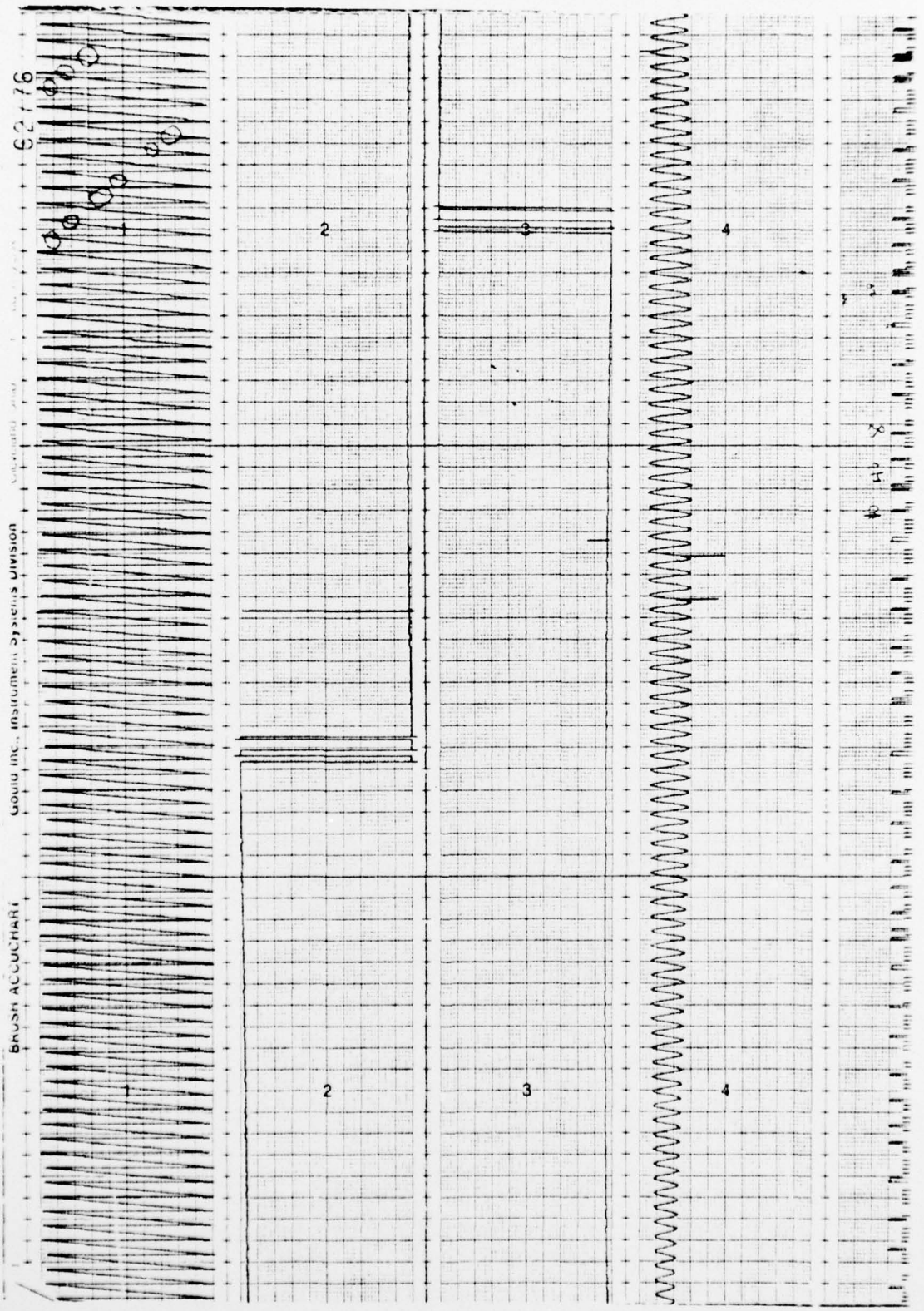
BRUSH ACCUCHART
Gould Inc., Instrument Systems Division
62.76
1
2
3
4

Figure 25

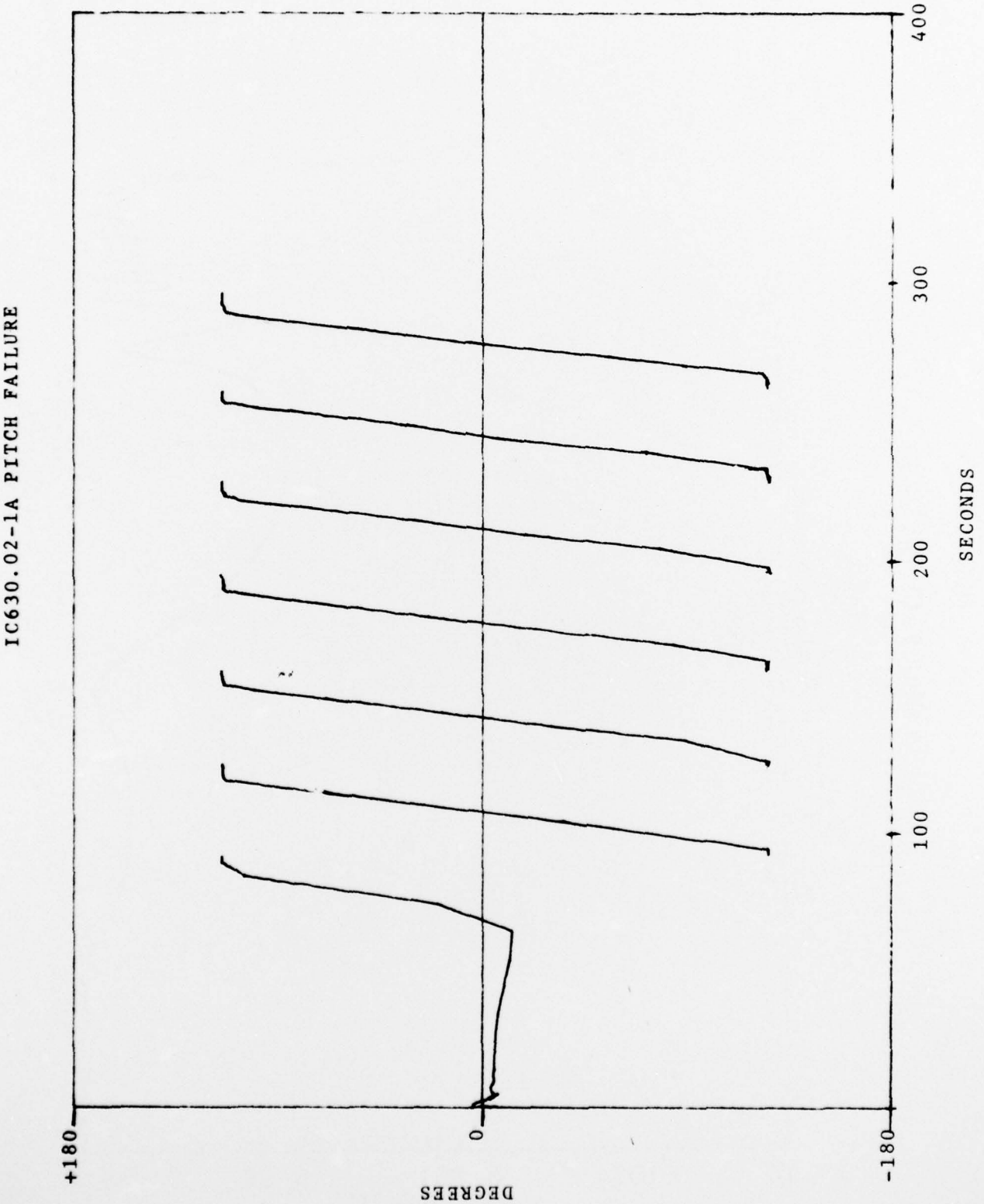
IC630.02-1A PITCH FAILURE
+180
0
-180
DEGREES
100
200
300
400
SECONDS

Figure 26

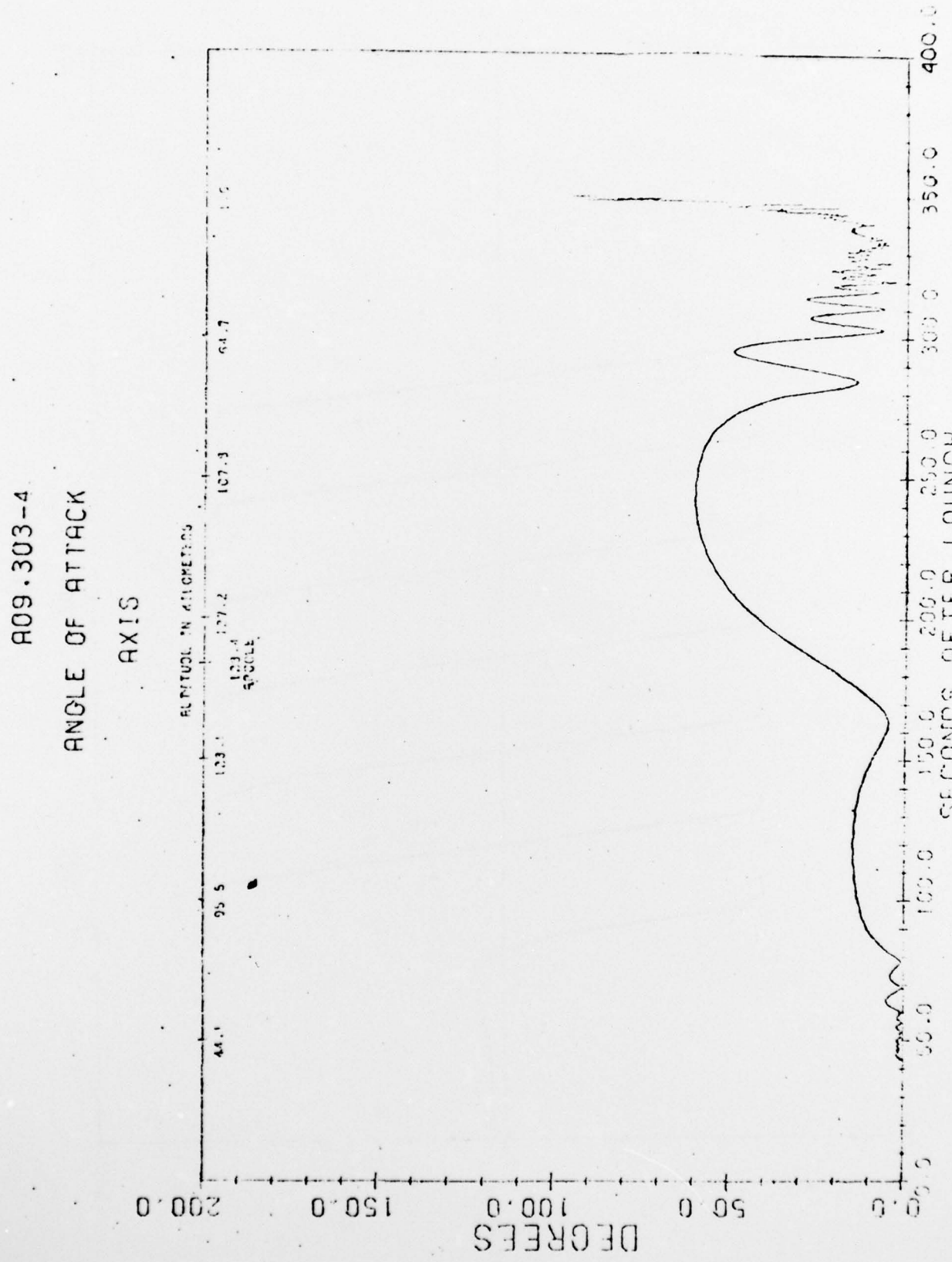

Figure 27

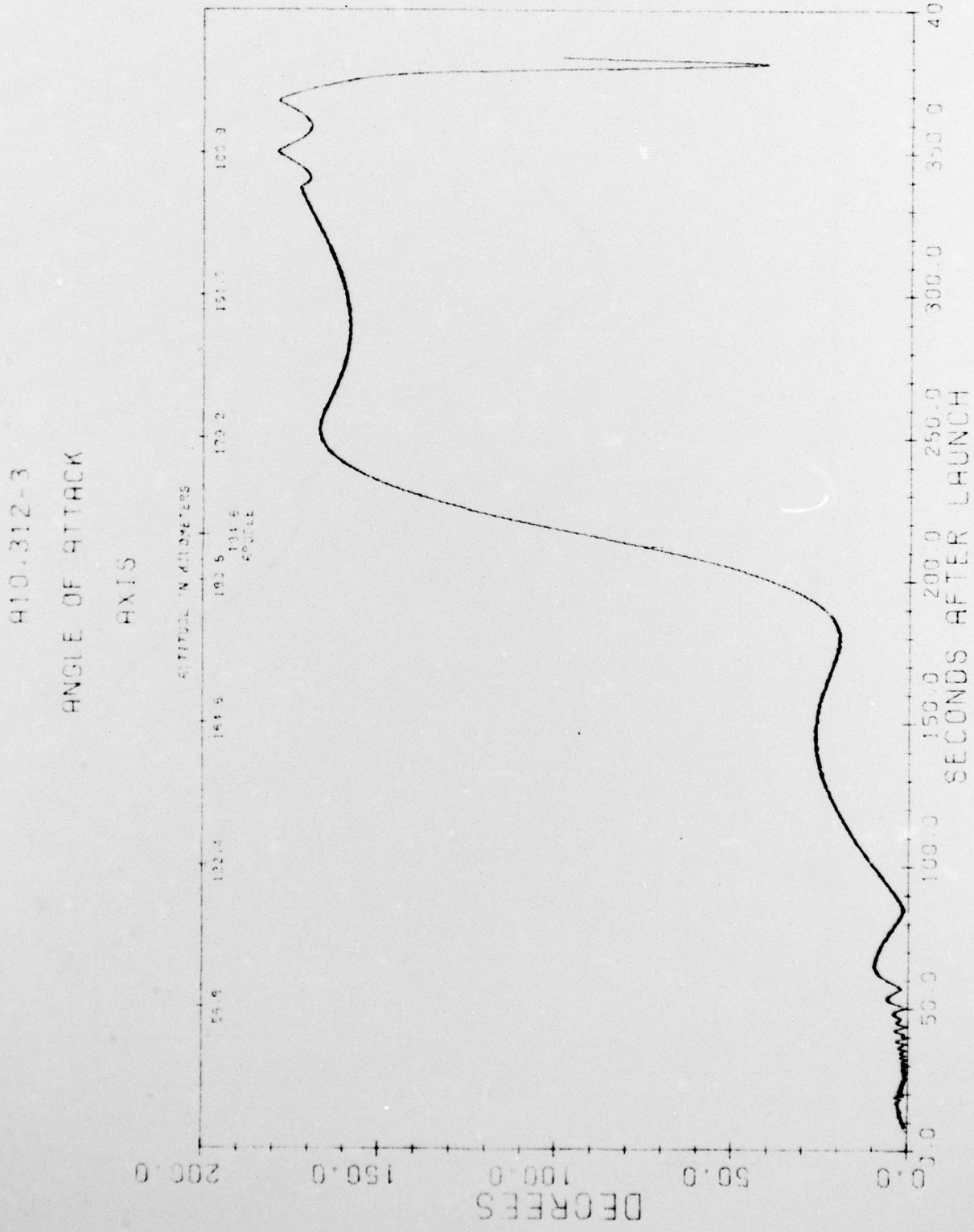

Figure 28

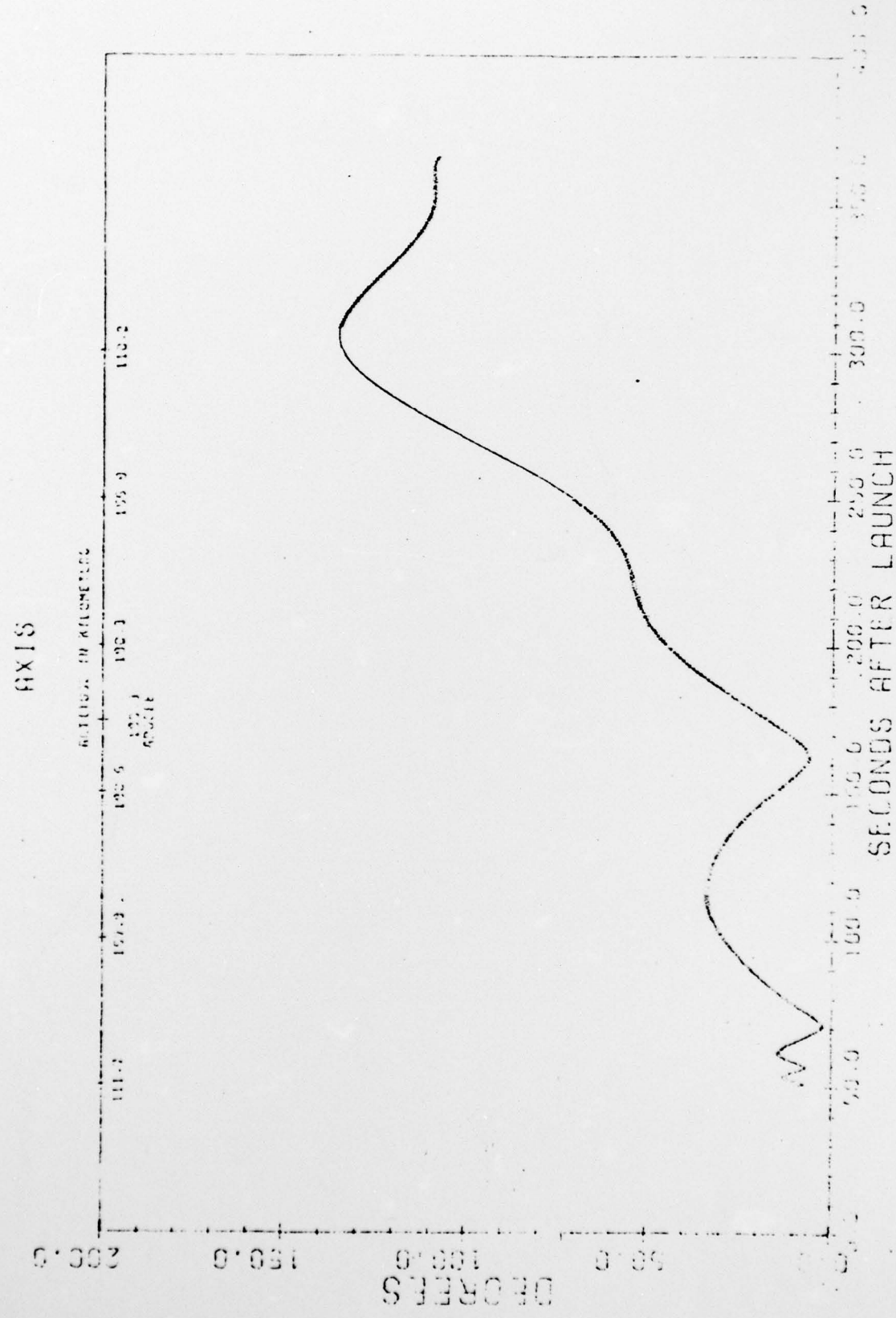
IC511.21A
ANGLE OF ATTACK
AXIS
SECONDS AFTER LAUNCH
DEGREES

REFERENCES

1. Daniel C., and Wood, F., Fitting Equations to Data, Wiley and Sons Inc., 1971.

2. Macon, N., Numerical Analysis, Wiley and Sons Inc., 1963.

3. Roxborough et al, Procedures for the Determination of the Attitude of a Rocket from Gyroscopic Data, Boston College, Final Report AFCRL-72-0740, prepared under Contract Number F19628-70-C-0017, September 1972.